

Transposon Mutagenesis in *Chlamydia trachomatis* Identifies CT339 as a ComEC Homolog Important for DNA Uptake and Lateral Gene Transfer

Scott D. LaBrie,^a Zoë E. Dimond,^a Kelly S. Harrison,^a Srishti Baid,^a Jason Wickstrum,^a Robert J. Suchland,^b P. Scott Hefty^a

^aDepartment of Molecular Biosciences, University of Kansas, Lawrence, Kansas, USA

^bDepartment of Medicine, University of Washington—Seattle, Seattle, Washington, USA

ABSTRACT Transposon mutagenesis is a widely applied and powerful genetic tool for the discovery of genes associated with selected phenotypes. *Chlamydia trachomatis* is a clinically significant, obligate intracellular bacterium for which many conventional genetic tools and capabilities have been developed only recently. This report describes the successful development and application of a *Himar* transposon mutagenesis system for generating single-insertion mutant clones of *C. trachomatis*. This system was used to generate a pool of 105 transposon mutant clones that included insertions in genes encoding flavin adenine dinucleotide (FAD)-dependent monooxygenase (*C. trachomatis* 148 [ct148]), deubiquitinase (ct868), and competence-associated (ct339) proteins. A subset of Tn mutant clones was evaluated for growth differences under cell culture conditions, revealing that most phenocopied the parental strain; however, some strains displayed subtle and yet significant differences in infectious progeny production and inclusion sizes. Bacterial burden studies in mice also supported the idea that a FAD-dependent monooxygenase (ct148) and a deubiquitinase (ct868) were important for these infections. The ct339 gene encodes a hypothetical protein with limited sequence similarity to the DNA-uptake protein ComEC. A transposon insertion in ct339 rendered the mutant incapable of DNA acquisition during recombination experiments. This observation, along with *in situ* structural analysis, supports the idea that this protein is playing a role in the fundamental process of lateral gene transfer similar to that of ComEC. In all, the development of the *Himar* transposon system for *Chlamydia* provides an effective genetic tool for further discovery of genes that are important for basic biology and pathogenesis aspects.

IMPORTANCE *Chlamydia trachomatis* infections have an immense impact on public health; however, understanding the basic biology and pathogenesis of this organism has been stalled by the limited repertoire of genetic tools. This report describes the successful adaptation of an important tool that has been lacking in *Chlamydia* studies: transposon mutagenesis. This advance enabled the generation of 105 insertional mutants, demonstrating that numerous gene products are not essential for *in vitro* growth. Mammalian infections using these mutants revealed that several gene products are important for infections *in vivo*. Moreover, this tool enabled the investigation and discovery of a gene critical for lateral gene transfer; a process fundamental to the evolution of bacteria and likely for *Chlamydia* as well. The development of transposon mutagenesis for *Chlamydia* has broad impact for the field and for the discovery of genes associated with selected phenotypes, providing an additional avenue for the discovery of molecular mechanisms used for pathogenesis and for a more thorough understanding of this important pathogen.

KEYWORDS *Chlamydia trachomatis*, genetic competence, mutagenesis, transposons

Citation LaBrie SD, Dimond ZE, Harrison KS, Baid S, Wickstrum J, Suchland RJ, Hefty PS. 2019. Transposon mutagenesis in *Chlamydia trachomatis* identifies CT339 as a ComEC homolog important for DNA uptake and lateral gene transfer. mBio 10:e01343-19. <https://doi.org/10.1128/mBio.01343-19>.

Editor Joanne Engel, University of California, San Francisco

Copyright © 2019 LaBrie et al. This is an open-access article distributed under the terms of the [Creative Commons Attribution 4.0 International license](https://creativecommons.org/licenses/by/4.0/).

Address correspondence to P. Scott Hefty, pshefty@ku.edu.

Received 24 May 2019

Accepted 28 June 2019

Published 6 August 2019

Transposon (Tn) mutagenesis is among the more effective strategies for discovering specific genetic components associated with a given phenotype. This genetic tool has been successfully applied for a better understanding of many basic biological processes as well as for the discovery of gene products associated with host infection and pathogenesis in diverse bacterial species (1, 2). Over a decade of optimization of naturally occurring transposon systems such as Sleeping Beauty and Tc1/*mariner* has resulted in a repertoire of successful genetic insertion systems.

One of the more widely applied transposons is the hyperactive form of the *Himar1 mariner* system (3). This variant has resulted in robust transposition efficiencies and has revolutionized the study of genotype-phenotype correlation (4). The *Himar* system has many benefits that have allowed applications in phylogenetically diverse bacteria (5–11), most importantly, the simplified “cut-and-paste” mechanism that requires a single transposase for recognition of inverted repeat sequences on flanking ends of DNA. This allows direct transposition of DNA to DNA, without the requirement of additional cofactors. Additionally, the *Himar* hyperactive transposase has minimal target DNA specificity, inserting between T/A nucleobases (7, 12) and allowing relatively nonspecific insertion across an entire genome (13–15). These advantages have proven beneficial for the study of pathogenesis in a diverse set of bacteria, including obligate intracellular organisms such as *Coxiella* and *Ehrlichia*. Research in *Coxiella* has demonstrated the use of *Himar1* Tn mutagenesis to identify genes critical for cellular growth and division *in vitro* (9, 10), whereas Tn studies in *Ehrlichia* revealed genes important for mammalian infection (8). Thus far, a transposon mutagenesis system has not been comprehensively described for the globally prevalent and obligate *Chlamydia* intracellular pathogens.

Chlamydia trachomatis is the most commonly reported cause of sexually transmitted bacterial infection in the United States and worldwide. *C. trachomatis* infections result in a range of health issues that include pelvic inflammatory disease, sterility, blindness, and pneumonia (16, 17). *C. trachomatis* contains a single, circular chromosome of ~1.04 Mb and a plasmid of ~7,500 bp (18, 19). Lateral gene transfer has likely played a critical factor in shaping chlamydial genomes. Moreover, lateral gene transfer occurs readily between strains, and genetic exchange between *C. trachomatis* genomes allows the interchange of polymorphic loci, such as the immunodominant major outer membrane porin gene (*ompA*), often resulting in enhanced tissue tropism and fitness against host defenses (20–26). Despite this key role, the components that participate in and the process involved in lateral gene transfer and DNA uptake are virtually unknown in *Chlamydia*. Similarly, many aspects of basic *C. trachomatis* biology and pathogenesis are poorly understood. This has been largely due to the limitations of the genetic tools that have been available for *Chlamydia*.

There has been a recent surge of introductions of molecular tools and methods developed for genetic manipulation in *Chlamydia* that has been enabled by the discovery of a transformation method and effective selectable antibiotic markers (27–32). TargetTron (29) and allele-specific recombination (33, 34) are two reverse genetic tools that have been developed for targeted gene disruption and have enormous potential for functional and phenotypic studies for candidate genes. However, only chemical mutagenesis has been developed for random and unbiased strategies (35–37). This method has been effectively employed to introduce multiple-base mutations, including nonsense mutations, allowing an association of gene products with noteworthy alterations to physiological pathways (36). While chemical mutagenesis is effective, it has certain limitations, including those represented by the acquisition of multiple mutations and the challenge of correlating a phenotype to a specific genetic disruption. Furthermore, identifying the mutations requires whole-genome sequencing (WGS) and revertant or compensatory mutations may be acquired during continued passaging. Thus, the development of a random single-insertion system, such as a *Himar1* transposon containing a selectable marker, allows straightforward generation of stable, single-site mutations and simplified identification of insertion sites.

Here, the development and application of a single-plasmid *Himar1* Tn system for *C.*

trachomatis are described. An initial subset of Tn insertion mutant strains was evaluated for potentially contrasting *in vitro* (tissue culture) and *in vivo* (mouse genital tract infection model) growth features. One of the transposon insertions occurred in a gene (*ct339*) that exhibits sequence similarity to that encoding an inner membrane DNA uptake protein termed ComEC. This mutant was investigated for the ability to perform lateral gene transfer and transformation-based DNA uptake.

RESULTS

Generation and genomic characterization of Tn insertion mutant clones using pCMA. A plasmid termed pCMA (plasmid *Chlamydia* Mariner) (see Fig. S1 in the supplemental material) was designed to encode the widely utilized C9 *Himar1* transposase (3). To reduce acquisition of deleterious mutations associated with plasmid propagation in *Escherichia coli*, the chlamydial *ct559* promoter and ribosomal binding site were cloned upstream of the C9 transposase. The *ct559* promoter has been characterized previously (38) and exhibited transcriptional activity in *Chlamydia* but limited activity in *E. coli*. The *bla* gene was cloned with flanking inverted repeats for recognition and transposition by the *Himar1* transposase. Finally, the plasmid contains only the *colE1* origin of replication for plasmid propagation in *E. coli*, which is non-functional in *Chlamydia*, resulting in a nonreplicative (suicide) vector upon transformation into *Chlamydia*.

The pCMA plasmid was used in a *C. trachomatis* transformation procedure with β -lactams for selection (39). This procedure typically requires three passages (i.e., infection-growth-lysis-reinfection) under conditions of antibiotic selection to ensure that the resulting organisms encoding β -lactamase (*bla*) are indeed able to form infectious progeny in the presence of β -lactams. In order to decrease the potential for normally growing mutants to outcompete fitness-compromised mutant clones in a mixed infection, as well as to evaluate transformation and transposon efficiency, transformation reactions (DNA and elementary bodies [EBs]) were mixed and incubated before being split into individual wells of a 12-well plate. Each well was passaged twice with selection, and after the second passage, cultures were allowed to continue growing, with daily monitoring of *C. trachomatis* growth. Within 2 days of cultivation, *C. trachomatis* growth was observed in approximately 4 of the 12 wells, although certain samples took longer than 2 days. A total of 23 transformations were performed with 105 resistant growth cultures and a range of 0 to 9 wells with resistant growth for each transformation. These observations suggest that the transformation efficiency in *C. trachomatis* is very low and/or that the genome may be less tolerant of transposon insertions. This efficiency was mirrored in five independent transformations performed with pGFP::SW2 which resulted in an average of 4.8 wells (range, 4 to 8) with resistant growth (data not shown), supporting the idea that transformation efficiency likely represents the limitation rather than transposon expression or function.

To identify the site(s) of transposon insertion and other potential mutations, whole-genome sequencing was applied to the 105 mutant strains as well as to the parental L2 strain (LGV 434/Bu Hefty; CP019386.1). All mutant strains contained a single transposon insertion in an expected insertion site (T/A). The absence of mixed Tn insertion strains supports the idea that clonal isolates were obtained following the distribution of transformation sample into individual 12 wells and multiple passaging with selection.

In total, 81 unique Tn insertion mutants were generated within coding regions (Fig. 1) (Table 1), with seven genes (*ct054*, *ct153*, *ct170*, *ct333*, *ct392*, *ct414*, and *ct550*) incurring transposon insertions in multiple sites of the coding region. While all of the studies were performed using *C. trachomatis* LGV 434/Bu, *C. trachomatis* serovar D gene nomenclature is utilized due to recognition and field familiarity. The gene *ct333* (*uvrA*) had 5 Tn insertions throughout the relatively large coding region (5,361 bp). Predominantly, Tn insertions resulted in the truncation of a protein-coding region with the addition of a short protein extension provided by the Tn insertion, depending on the insertion site and reading frame. Most of these insertions were found to have occurred

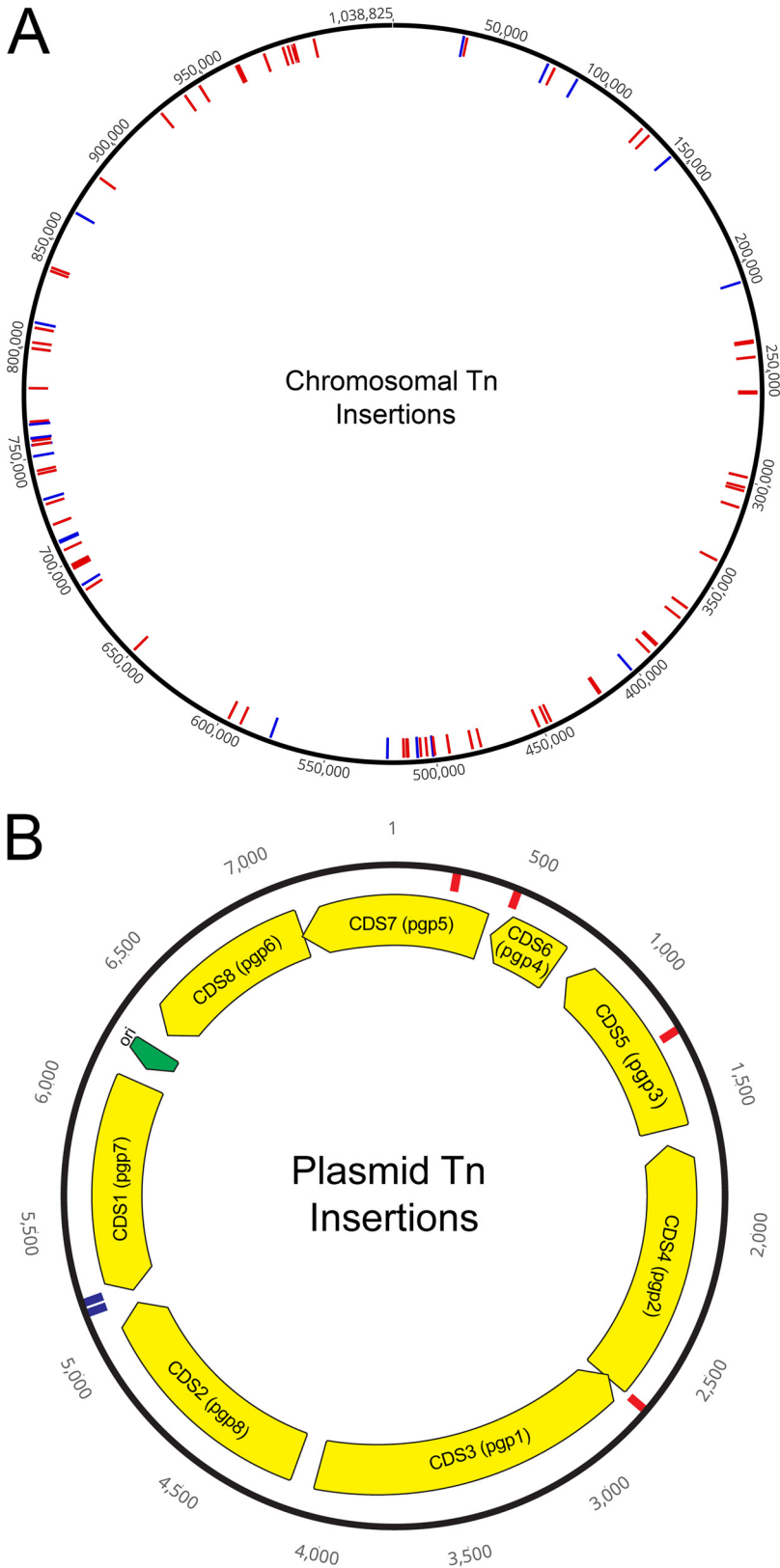


FIG 1 Map of transposon insertions in *C. trachomatis* chromosome and plasmid. (A) Sites of transposon insertions within coding regions (red) and noncoding regions (blue) throughout the *C. trachomatis* L2 434/Bu chromosome. (B) Sites of transposon insertions within the coding regions (red) and noncoding regions (blue) throughout the *C. trachomatis* L2 434/Bu plasmid. ori, origin of replication.

TABLE 1 C. trachomatis coding region transposon insertion mutants

ctl gene (ct):Tn bla	Gene name	Predicted function	Genomic position of TN insertion ^a	Gene insert site/total gene length (bp)	Modified protein sequence ^d	Sequence modification [truncated/normal length] (bp) ^d
ctI0027 (ct658)	<i>sfhB</i>	Pseudouridine synthase	33827	544/1,008	QVKK LX	[Y182X; 182/335]
ctI0063 (ct694)		Hypothetical	76200	17/969	SIRPTNRLDDKSPV X	[G8R; 16/322]
ctI0065 (ct696) ^e		Hypothetical	79522	1,039/1,179	MRVLL X	[M347X; 346/392]
ctI0101 (ct732) ^e	<i>ribH</i> (<i>ribE</i>)	6,7-Dimethyl-8-ribityllumazine synthase	124470	44/474	KDVRVITGWMISPRSDAQW NSRX	[A16T; 34/157]
ctI0105 (ct736)		Hypothetical phosphatidyl ethanolamine-binding proteins	129068	191/453	WIHWITGWMISPRSDAQW NSRX	[V65T; 83/150]
ctI0125	<i>murF</i>	UDP-N-acetylmuramoyl-tripeptide- α -alanine- β -alanine ligase	159474	1,328/1,353	ELELITGWMISPRSDAQW NSRX	[L404T; 462/450]
ctI0175 (ct806) ^h	<i>ptr</i>	Periplasmic Zn-dependent peptidase	223999	1,236/2,871	INSLEYNRLDDKSPV X	[S422X; 422/957]
ctI0184 (ct813) ^h		Inclusion membrane protein	235508	355/795	OFRIVITGWMISPRSLVAQR-35AA-YF X	[M120T; 171/264]
ctI0185 (ct814) ^e		Hypothetical membrane-associated protein	236256	74/300	FGGFLITGWMISPRSDAQW NSRX	[A26T; 44/99]
ctI0191 (ct819)		yccA-BAX inhibitor	242990	121/717	TSLGL X	[Y41X; 41/238]
ctI0201 (ct829)		tRNA [guanine-N(7)-l-methyltransferase	258702	68/675	IANHVTGWMISPRSDAQW NSRX	[F24T; 42/224]
ctI0202 (ct830)		Putative SAM-dependent methyltransferase	259440	17/585	MLTGITGWMISPRSDAQW NSRX	[D7T; 16/194]
ctI0238b		Hypothetical	298245	184/306	PYQYD X	[Y62X; 62/101]
ctI0246 (ct867)	<i>cdv2</i>	Deubiquitinase and deneddylase	302887	877/1,020	OFLAW X	[Y293X; 293/339]
ctI0247 (ct868)	<i>cdv1</i>	Deubiquitinase	304303	889/1,206	DSL YNX	[N297X; 297/401]
ctI0250 (ct871)	<i>pmpG</i>	Polymorphic outer membrane protein	312316	786/3,039	HPTCYFNRRSSSKFFQKYCGRV X	[G738F; 755/1,012]
ctI0270 (ct015)		Phosphate-responsive ATPase, PhoH-like protein	338386	1,277/1,305	ERSELTGWMISPRSDAQW NSRX	[A427T; 445/434]
ctI0291 (ct036) ^h		Hypothetical, putative Inc	363864	620/1,158	LQQLITGWMISPRSDAQW NSRX	[D208T; 226/385]
ctI0298 (ct042) ^h		Putative glycosyl hydrolase	369458	681/2,001	PSRRYRRLDDKSPV X	[T228N; 237/666]
ctI0310 (ct054) ^h	<i>sucA</i>	2-Oxoglutarate dehydrogenase E1 component	385356	2,122/2,712	ARIER X	[Y708X; 708/903]
ctI0314 (ct054) ^h	<i>sucA</i>	2-Oxoglutarate dehydrogenase E1 component	385932	2,699/2,712	TLFSITGWMISPRSDAQW NSRX	[G901T; 919/903]
ctI0319 (ct058)		Putative membrane-spanning protein	390466	401/1,092	GWNCTITGWMISPRSDAQW NSRX	[E135T; 153/363]
ctI0339 (ct084)		Phospholipase D superfamily	419045	827/1,086	HOIQLITGWMISPRSDAQW NSRX	[H277T; 295/361]
ctI0343 (ct088)	<i>ssc1</i>	Type III secretion chaperone	423934	413/441	ELPDLITGWMISPRSDAQW NSRX	[H139T; 157/146]
ctI0361 (ct106) ^h		tRNA pseudouridine synthase A	445244	626/825	LEKDGRLDDKSPV X	[K364N; 373/368]
ctI0362 (ct107)		A/G-specific adenine glycosylase	447004	1,089/1,107	TSSAPNRLDDKSPV X	[M590N; 599/608]
ctI0367 (ct112)	<i>pepF</i>	Oligoendopeptidase F	450974	1,767/1,825	AWEHTRRLDDKSPV X	[K113N; 122/427]
ctI0394 (ct139) ^h	<i>oppA</i>	Oligopeptide transport system binding protein	479190	336/1,281	TSLSYRRLDDKSPV X	[I237N; 246/280]
ctI0398 (ct143)		Hypothetical	482984	708/843	GINLANRLDDKSPV X	[K389N; 398/663]
ctI0401 (ct146)	<i>lga</i>	NAD-dependent DNA ligase	487189	1,164/1,992	TPKW LX	[I163X; 163/507]
ctI0403 (ct148)	<i>nphA</i>	FAD-dependent monooxygenase	493563	487/1,524	PPGTLTGWIMISPRSDAQW NSRX	[R223X; 223/811]
ctI0408 (ct153)	<i>macP</i>	Membrane attack complex	499954	611/2,433	SIDSDNRLDDKSPV X	[R29N; 38/811]
ctI0408 (ct153)	<i>macP</i>	Membrane attack complex	500482	84/2,433	KESAHNRLDDKSPV X	[T320N; 329/401]
ctI0413 (ct157)		Phosphatidylcholine-hydrolyzing phospholipase D	504003	956/1,206	MOGAY X	[Y39X; 39/93]
ctI0417a (ct159)		Hypothetical	506473	118/282	VNQALITGWMISPRSLVAQR-35AA-YF X	[Q172T; 223/392]
ctI0423 (ct170)	<i>trpB</i>	Tryptophan synthase, beta subunit	512551	512/1,179	FFHFNRRLDDKSPV X	[I242N; 251/392]
ctI0423 (ct170)	<i>trpB</i>	Tryptophan synthase, beta subunit	512763	723/1,179	VPVLITGWMISPRSDAQW NSRX	[A200T; 218/398]
ctI0496 (ct244) ^h		Hypothetical	591198	596/1,197	EGQELITGWMISPRSDAQW NSRX	[R283T; 301/814]
ctI0500 (ct248)	<i>glgP</i>	Alpha-1,4 glucan phosphorylase	596937	845/2,445	ISSNITGWMISPRSDAQW NSRX	[I144T; 162/454]
ctI0550 (ct298) ^h	<i>radA</i>	DNA repair protein	650265	429/1,365	FFVITGWMISPRSDAQW NSRX	[S168T; 186/515]
ctI0578 (ct326)		Hypothetical	685322	670/1,545	VSIPLITGWMISPRSDAQW NSRX	[G618T; 636/1,786]
ctI0587 (ct333) ^h	<i>uvrA</i>	UvrABC system protein A	696123	1,850/5,361	ELPVLITGWMISPRSDAQW NSRX	[P925T; 943/1,786]
ctI0587 (ct333) ^h	<i>uvrA</i>	UvrABC system protein A	697044	2,771/5,361	LNHES X	[Y1201X; 1,201/1,786]
ctI0587 (ct333) ^h	<i>uvrA</i>	UvrABC system protein A	697874	3,601/5,361	ESLCLITGWMISPRSDAQW NSRX	[G1274T; 1,292/1,786]
ctI0587 (ct333) ^h	<i>uvrA</i>	UvrABC system protein A	698091	3,818/5,361	LDEIANRLDDKSPV X	[T1723N; 1,732/1,786]
ctI0587 (ct333) ^h	<i>uvrA</i>	UvrABC system protein A	699439	5,165/5,361		

(Continued on next page)

TABLE 1 (Continued)

ctI gene (ct ^r ::Tn bla)	Gene name	Predicted function	Genomic position of TN insertion ^a	Gene insert site/total gene length (bp)	Modified protein sequence ^d	Sequence modification [truncated/normal length] (bp) ^d
ctI0593 (ct339) ^h	<i>comEC</i>	Competence DNA uptake	705937	1,466/1,530	ILVYITGWMISPRSDAQWNNRSRX	[R61T; 508/509]
ctI0604 (ct350)		Putative lipoprotein	718288	179/1701	IQPVTRNSRVFTTKLSLIX	[R61T; 79/566]
ctI0611A (ct357) ^h		Hypothetical	728274	212/333	DFSVLTGWMISPRSDAQWNNRSRX	[R61T; 90/110]
ctI0625 (ct371)		Putative outer membrane protein	742559	454/786	KANLPLTGWIMISPRSDAQWNNRSRX	[Y152L; 171/261]
ctI0626 (ct372) ^h	<i>aaxA</i>	Porin	743881	837/1,329	KWSNLNRLDDKSPVX	[T280N; 289/442]
ctI0639 (ct383)		Putative inner membrane protein	758828	572/732	ERYTLTGWIMISPRSDAQWNNRSRX	[L192T; 210/243]
ctI0641 (ct385)		Histidine triad motif hydrolase	757770	198/336	EAGKINRLDDKSP-35AA-SCX ^g	[I67N; 112/111]
ctI0648 (ct392) ^h		Hypothetical	765648	762/1,131	DGPLSNRLDDKSPVX	[S300X; 300/377]
ctI0648 (ct392) ^h		Hypothetical	766400	11/1,131	MSSITGWIMISPRSDAQWNNRSRX	[Q5T; 23/376]
ctI0661 (ct404)		N6-adenine-specific DNA methylase	781874	690/828	HTPGHNRLDDKSPVX	[T231N; 240/275]
ctI0671 (ct414) ^h	<i>pmpC</i>	Polymorphic outer membrane protein	799909	1,559/5,325	TNSDTGWMISPRSDAQWNNRSRX	[D521T; 539/1,774]
ctI0671 (ct414) ^h	<i>pmpC</i>	Polymorphic outer membrane protein	802592	4,241/5,326	APQKGYNRLDDKSPVGSSENLR	[Q1460X; 1,460/1,775]
ctI0671 (ct414) ^h	<i>pmpC</i>	Polymorphic outer membrane protein	802593	4,242/5,326	PQKGYNRLDDKSPVX	[S1455N; 1,424/1,774]
ctI0678 (ct421)		Hypothetical	804491	686/702	TSPFITGWIMISPRSDAQWNNRSRX	[L444T; 462/450]
ctI0707 (ct447)	<i>recJ</i>	Single-stranded DNA-specific exonuclease	836380	1,311/1,755	DFAAGLNRLDDKSPVX	[M438L; 447/584]
ctI0708a (ct448)		Bifunctional preprotein translocase subunit <i>secDF</i>	838006	4,005/4,203	EQKTLTGWIMISPRSDAQWNNRSRX	[G1337T; 1,355/1,400]
ctI0730 (ct470)	<i>recO</i>	DNA repair protein	863604	492/732	ESSTIX	[Y165X; 165/244]
ctI0750 (ct489)	<i>glgC</i>	Glucose-1-phosphate adenylyltransferase	884304	469/1,326	RSIVDX	[Y157X; 157/441]
ctI0802 (ct540)		Putative tRNA [cytidine(34)-2'-O]-methyltransferase	925001	418/456	VGIVMX	[Y140X; 140/151]
ctI0812 (ct550)		Hypothetical	938483	42/426	FRRSNRLDDKSPVX	[T15N; 24/141]
ctI0818 (ct555) ^e		ATP-dependent helicase	946408	3,260/3,600	FIGSLTGWIMISPRSDAQWNNRSRX	[L1088T; 1,106/1,199]
ctI0837 (ct574) ^e	<i>pepP</i>	Aminopeptidase P family protein	965163	87/1,071	KDEDINRLDDKSPVX	[S30N; 39/356]
ctI0838 (ct575) ^{eh}	<i>mutL</i>	DNA mismatch repair endonuclease	966365	626/1,731	KOGFTGWIMISPRSDAQWNNRSRX	[E210T; 228/576]
ctI0849 (ct586)	<i>uvrB</i>	Excinuclease ABC subunit B	979090	848/2,007	EGRPVTGWIMISPRSDAQWNNRSRX	[E284T; 302/668]
ctI0853 (ct590) ^h		Hypothetical	986413	2,164/2,865	DKSAIK	[I122X; 722/955]
ctI0853 (ct590) ^h		Hypothetical	988197	380/2865	RVQDITGWIMISPRSDAQWNNRSRX	[I128T; 145/954]
ctI0855 (ct592)	<i>sdhA</i>	Succinate dehydrogenase flavoprotein	990457	875/1,881	PWYFLTGWIMISPRSDAQWNNRSRX	[E293T; 311/626]
ctI0856 (ct593) ^e	<i>sdhC</i>	Succinate dehydrogenase	992076	114/862	HLITNRLDDKSPVX	[I39N; 48/287]
ctI0858 (ct594)	<i>tatD</i>	Hydrolase	992950	178/792	DWMFYNRLDDKSPVX	[H61N; 69/261]
ctI0867 (ct604)	<i>groEL2</i>	Molecular chaperone GroEL	1002459	431/1,602	LEHTVX	[Y144V; 144/533]
ctI_r03/04		23S rRNA	136240 OR 158284	404/2,868		
ctI0425 (ct172)		Pseudogene	514407			
CDS7 (<i>pgp5</i>)	<i>pgp5</i>	Plasmid hypothetical protein	229 ^b	165/795	SGLGANRLDDKSPVX	[S52N; 61/264]
CDS6 (<i>pgp4</i>)	<i>pgp4</i>	Plasmid hypothetical protein	460 ^b	270/309	ALIMLNRLDDKSPVX	[I91N; 100/102]
CDS5 (<i>pgp3</i>)	<i>pgp3</i>	Plasmid virulence protein	1262 ^b	331/795	ALIMLNRLDDKSPVX	[I91N; 100/102]
CDS3 (<i>pgp1</i>)	<i>pgp1</i>	Plasmid helicase	2715 ^b	1,354/1,356	IKKVVX	[K451X; 451/451]
CDS4 (<i>pgp2</i>)	<i>pgp2</i>	Plasmid hypothetical protein	2715 ^b	5/1,065	MVYTGWMISPRSDAQWNNRSRX	[N6M; 21/354]

^aPosition generated using *C. trachomatis* LGV 434/Bu (NC_010287).^bPosition generated using *C. trachomatis* LGV 434/Bu plasmid (NC_021051.1).^c*C. trachomatis* serovar D (NC_000117) gene nomenclature.^dHimar insertion delineated by underscore; first amino acid shift delineated by bold highlighting and shown in square brackets; stop codon delineated by X. Data were calculated as follows: (protein length after insertion)/(wild-type protein length).^eSlow-growing mutants (mutants that required six or more passages to achieve visibly infectious stocks).^fComplete C-terminal sequence, QFRIVTGWIMISPRSLVAQRTEKPKCKAVFSEGEITRRPKRSEQEDHLVNIQKIFYX.^gComplete C-terminal sequence, EAGKINRLDDKSPVGSSENLRKALQGGFFVFRARDYAQTKTISRSSCX.^hDenotes coding regions that were shared as nonsense mutants as reported previously by Kokes et al. (36).

within the first 60% of the coding region, providing higher confidence that the Tn insertion is disruptive to the normal protein function. Four of the insertions (*ct015::Tn*, *ct054::Tn*, *ct088::Tn*, and *ct107::Tn*; Table 1) extended the normal protein sequence, which may have little effect on protein function. Sixteen of the Tn insertions occurred in hypothetical proteins, while the rest occurred in a variety of genes with contributions to diverse biological functions. For example, five Tn insertions (*ct298*, *ct333*, *ct470*, *ct586*, and *ct575*) were involved in DNA repair mechanisms, four (*ct054*, *ct248*, *ct489*, and *ct592*) were involved in central metabolism, and four (*ct404*, *ct540*, *ct829*, and *ct830*) encoded methyl modification enzymes. Two polymorphic membrane protein-coding regions (*ct871* [*pmpG*] and *ct414* [*pmpC*]) incurred insertions, as did both deubiquitinases (*ct867* [*cdu2*] and *ct868* [*cdu1*]). Of note, 16 of the Tn insertions occurred in genes that also incurred nonsense mutations following chemical mutagenesis (36), for a total of 54 new gene disruptions generated.

Twenty-three mutant strains had Tn insertions within an intergenic region (Table 2). Many of these insertions occurred between genes with divergent coding directions as well as between those with shared coding directions, both of which could result in disruptions to gene expression. Insertions upstream of eight (*ct690*, *ct792*, *ct793*, *ct182*, *ct328*, *ct343*, *ct387*, and *ct472*) of the diverging genes occurred within 80 nucleotides (nt) of start codons. On the basis of the determinations of transcriptional start sites located on average 50 nt upstream of start codons (40) and promoters covering at least an additional 50 nt, these Tn insertions likely disrupt transcription initiation and gene expression. For insertions between genes with shared coding directions, three (*ct343*, *ct373*, and *ct423*) have transcriptional start sites reported upstream of or near (within 40 nt) the insertion potentially disrupting gene expression. Three Tn insertions also occurred between genes with convergent coding directions. While the possibility of disruption of gene expression (effecting termination or noncoding RNAs [ncRNAs]) cannot be ruled out, it is less likely that these flanking genes are affected by these Tn insertions.

Tn insertions also occurred within the chlamydial plasmid. Four (*pgp1*, *pgp2*, *pgp4*, and *pgp5*) of the coding regions incurred an insertion, although the Tn insertion in *pgp1* was at the second to last codon and may have little effect on the protein generated. Two Tn insertions were also found in the intergenic region of the convergent *pgp7* and *pgp8* genes. Two prior studies have investigated the requirement of individual genes for plasmid maintenance (41, 42). Both studies supported the idea that products of the *pgp1*, *pgp4*, and *pgp5* genes are not required; however, the presence of almost all of the *pgp2* coding region was found to be required for plasmid maintenance. As such, it was unexpected for a Tn insertion in *pgp2* which results in a severely truncated coding region to be identified. This may indicate that there is a product (e.g., ncRNA) within the coding region, instead of the expected Pgp2 protein product, that is key for plasmid replication. In support of this, the *pgp2::Tn* mutant strain was grown without antibiotics for two passages and the plasmid was found to still be present by PCR analysis (data not shown).

In vitro growth characteristics of transposon mutants. While most of the transposon mutant clones did not exhibit noticeably slow growth or poor production of infectious progeny during initial selection and tissue culture propagation, more-subtle growth rates or morphologic differences may be associated with certain mutants. To discover potential defects in infection, growth, or developmental cycle processes associated with transposon mutant clones, temporal analyses of infectious progeny production and bacterial morphologies and quantitative assessment of inclusion sizes were performed for a subset of 16 Tn mutants (Fig. 2; see also Fig. 3 and Fig. S2 and S3). In addition to the parental strain, a clone with a Tn insertion between converging genes (*ct383/4::Tn*) was also evaluated.

Analyses of the production levels of infectious progeny (EB) of parental (wild-type [WT]) and individual Tn mutant clones were performed on lysates in 6-h increments between 18 and 42 h postinfection (hpi) (Fig. 2). Progeny production levels reflect

TABLE 2 C. trachomatis intergenic region transposon insertion mutants

Flanking CTL genes (CT):Tn bla	Flanking gene orientation	Genomic position of TN insertion ^a	Gene insert site/total gene length (bp)	Potential gene function disruption
ct10024/0025 (ct655/656)	Converging	32332		
ct10059/0060 (ct690/691)	Diverging	72505	50/110 nt upstream of <i>dppD/phoU</i>	<i>dppD</i> (oligopeptide ABC transporter ATP-binding protein) and <i>phoU</i> (phosphate transport)
ct10070/0071 (ct701/702)	Converging	87381		
ct10111/0112 (ct742/743)	Shared direction	142632	98 nt upstream of <i>trmA</i> (CTL0111)	<i>trmA</i> ; 23S rRNA (uracil-5-)-methyltransferase
ct10160/0162 (ct792/793)	Diverging	208013	57/12 nt upstream of <i>mutS</i> /hypothetical	<i>mutS</i> ; DNA mismatch repair protein
ct10322/0323 (ct076/077)	Diverging	401583	176/484 upstream of hypothetical/ <i>troA</i>	
ct10339/0340 (ct084/085)	Shared direction	419884	13 nt upstream of CTL0339	CTL0339; Phospholipase D
ct10408/0411 (ct154)	Shared direction	501211	646 nt upstream of CTL0408	
ct10417/0418 (ct161/162)	Shared direction	508108	56 nt upstream of hypothetical (CTL0417)	
ct10433/0434 (ct181/182)	Diverging	522045	287/80 nt upstream of hypothetical/ <i>kdsB</i>	<i>kdsB</i> ; CMP-2-keto-3-deoxyoctulosonic acid synthetase
ct10482/0483 (ct230/231)	Shared direction	576139	134 nt upstream of <i>yocR</i> (CTL0483) ^d	<i>yocR</i> ; Sodium-dependent transporter
ct10581/0582 (ct327/328)	Diverging	687877	161/34 nt of <i>trpC</i> / <i>tpiA</i>	<i>trpC</i> (phosphoribosylanthranilate isomerase) and <i>tpiA</i> (triosephosphate isomerase)
ct10596/0597 (ct342/343) ^e	Shared direction	709636	110 nt upstream of <i>rpsU</i> ^d	<i>rpsU</i> ; S21 ribosomal protein
ct10597/0598 (ct343/344)	Diverging	710369	13/297 nt upstream of <i>tsaB</i> / <i>lon</i>	<i>tsaB</i> ; tRNA threonylcarbamoyladenosine modification protein
ct10614/0615 (ct360/361)	Shared direction	730550	67 nt upstream of hypothetical	
ct10633/0634 (ct378/379)	Shared direction	750823	53 nt upstream <i>pgi</i> ^d	
ct10639/0640 (ct383/384)	Converging	755990		
ct10642/0643 (ct386/387)	Diverging	759051	218/69 nt upstream of hypothetical proteins	
ct10647/0648 (ct391/392)	Converging	765276		
ct10682/0683 (ct423/424)	Shared direction	811934	25 nt upstream of <i>rsbV</i> (CTL0683)	<i>rsbV</i> ; anti-sigma factor antagonist
ct10731/0733 (ct471/472)	Diverging	864902	460/18 upstream of hypothetical proteins	
CDS1/2 (<i>pgp7/8</i>)	Converging	5189 ^b		
CDS1/2 (<i>pgp7/8</i>)	Converging	5232 ^b		

^aPosition generated using C. trachomatis LGV 434/Bu (NC_010287).^bPosition generated using C. trachomatis LGV 434/Bu plasmid (NC_021051.1).^cC. trachomatis serovar D (NC_000117) gene nomenclature.^dTranscription start site reported (40) upstream of coding region.^eSlow-growing mutants (mutants that required six or more passages to achieve visibly infectious stocks).

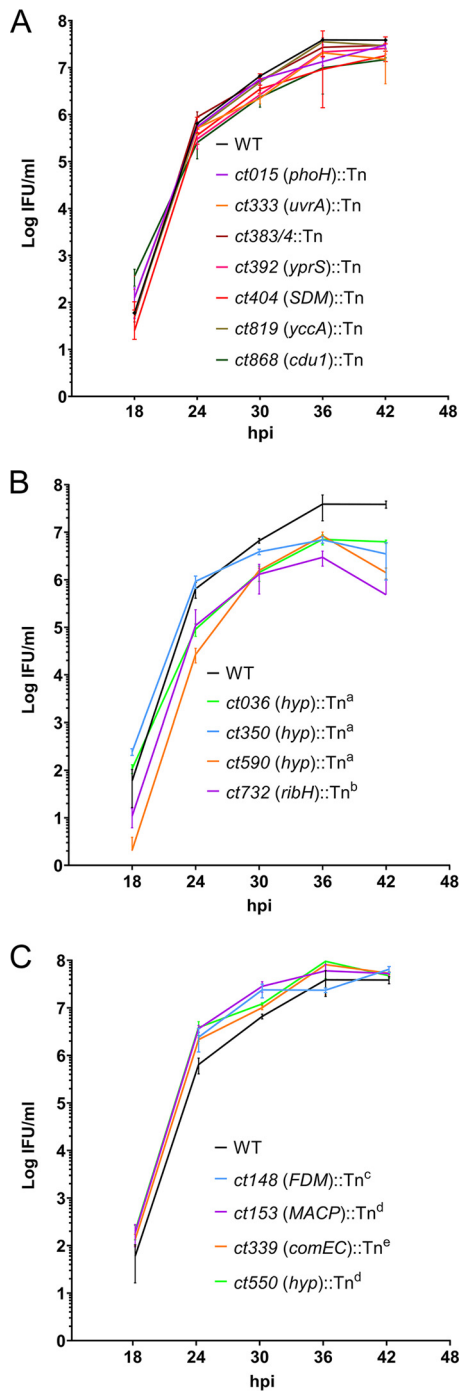


FIG 2 Progeny production of Tn mutants from 18 to 42 hpi. L929 cells were infected with the WT (parental) strain or a Tn insertion mutant clone (gene with Tn insertion is indicated) in triplicate. Quantities of inclusion-forming units (IFU) were determined from lysates at 18, 24, 30, 36, and 42 hpi. Mutants showed progeny production patterns similar to those of the WT parental L2 clone (A), those with significantly decreased progeny production at multiple time points (B), or those with significantly enhanced progeny production at one or more time points (C). Data are shown as means and SD of results from triplicate wells. Statistical significance was calculated using Student's two-tailed unpaired *t* test with a *P* value of <0.05. Progeny production was significantly reduced at 24, 30, and 42 hpi (indicated with a superscript "a") or at 24, 30, 36, and 42 hpi (indicated with a superscript "b"). Progeny production was significantly increased at 30 and 42 hpi (indicated with a superscript "c") or 24 and 30 hpi (indicated with a superscript "d") or 24, 30, and 42 hpi (indicated with a superscript "e").

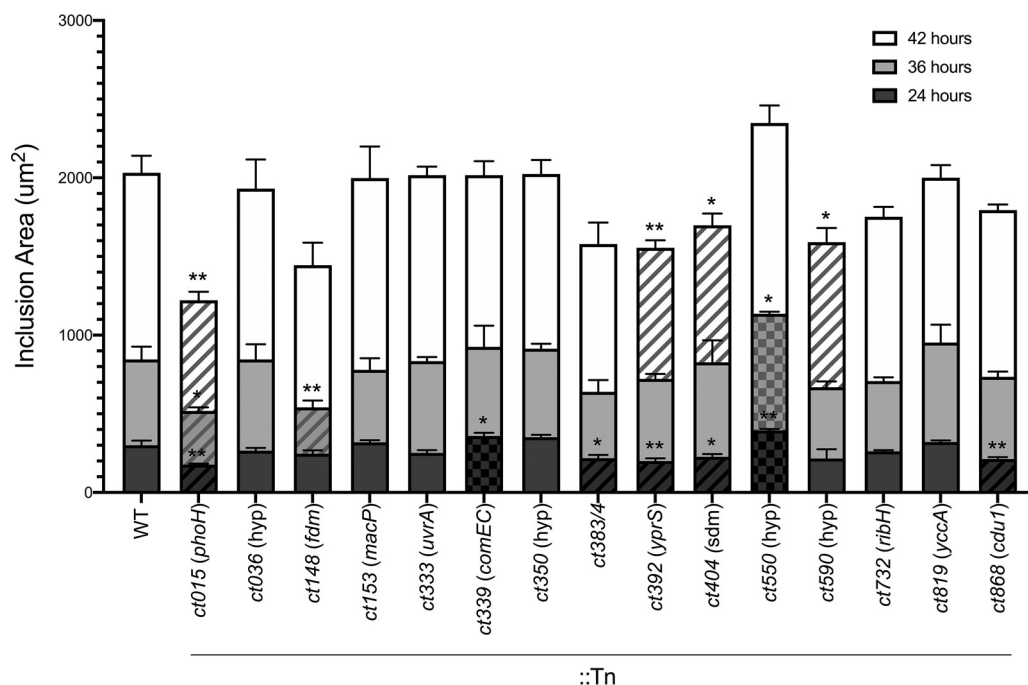


FIG 3 Inclusion sizes of Tn mutant strains. Inclusion size was measured at 24, 36, and 42 h postinfection for each Tn mutant and parental strain (WT). Mutant strains are displayed as stacked bars showing inclusions larger than the WT inclusions (checked), equal to the WT inclusions in size (solid), or smaller than the WT inclusions (striped). Triplicate samples were evaluated, with 250 to 1,000 inclusion areas measured per sample. **, $P < 0.005$; *, $P < 0.05$ (unpaired Student's *t* test).

bacterial replication as well as ability to convert into the infectious EB form. Defects in either of these can be detected with this approach, enabling a more focused analysis of candidate mutant strains. Three distinct growth phenotypes were observed among Tn mutants; normal, decreased, and increased progeny production relative to the parent strain. Almost half (7 of 16) of the Tn mutants displayed EB production levels and timing similar to those seen with the WT, as did the clone with a Tn insertion between two converging genes (*ct383/4::Tn*) (Fig. 2A). However, four mutants (*ct036::Tn*, *ct350::Tn*, *ct590::Tn*, and *ct732::Tn*) displayed significant deficiencies in progeny production at two or more time points (Fig. 2B). At 24 hpi, strain *ct590::Tn* (hypothetical) displayed progeny production levels that were almost 2 log-fold lower whereas *ct036::Tn* and *ct732::Tn* (*ribH*) mutants displayed progeny production levels that were about 1 log-fold lower. An interesting observation was the enhanced progeny production of four mutant clones (*ct153::Tn*, *ct148::Tn*, *ct339::Tn*, and *ct550::Tn*), which was most notable at 24 hpi. Clones *ct153::Tn* and *ct148::Tn* maintained this enhanced level at 30 hpi, with all of the mutant clones matching the parental clone at 36 and 42 hpi (Fig. 2C). Of the Tn mutants evaluated, *ct696::Tn* displayed the most contrasting and slowest growth phenotype, with propagation requiring up to 5 days before passage was successful and with undiluted cell lysate and levels of inclusion-forming units (IFU) below 10/ml (data not shown). Overall, progeny production analysis revealed that defects were observed for many of the Tn insertion clones, albeit most of the data were within a log-fold difference range.

Defects in the temporal expansion of an inclusion could suggest that a gene product plays a role in many aspects of chlamydial growth, and so, the area of inclusions was calculated at 24, 36, and 42 hpi. The data shown in Fig. 3 highlight that the inclusions for 5 Tn mutants (*ct015::Tn*, *ct383/4::Tn*, *ct392::Tn*, *ct404::Tn*, and *ct868::Tn*) were significantly smaller than that for the parental strain at 24 hpi. Only mutant *ct015::Tn* maintained smaller inclusion sizes at 36 and 42 hpi, with *ct392::Tn*, *ct404::Tn*, and *ct590::Tn* displaying smaller inclusions at 42 hpi. Two Tn mutants (*ct339::Tn* and *ct550::Tn*) had inclusions larger than the parental inclusions at 24 hpi, with the *ct550::Tn*

inclusions maintaining a larger size than the parental inclusions at 36 hpi. Interestingly, *ct550::Tn* was the only mutant to display a correlation between progeny production and inclusion size (Fig. 2C; see also Fig. 3), both of which showed increases relative to the parental data.

To discover if any abnormal morphologic phenotypes (bacterial or inclusion) are associated with this subset of transposon mutant clones, confocal microscopy was applied to immunostained parental and transposon mutants at 24, 36, and 42 hpi (Fig. S2). Almost all of the Tn mutants displayed inclusions that were localized near the nucleus as well as general shapes of the inclusion and reticulate bodies (RBs) that were similar to those seen with the parental strain. Notable exceptions included mutant *ct048::Tn*, which contained larger but fewer RBs within the inclusion at 42 hpi. Similarly to the growth assessments, the *ct696::Tn* inclusions and bacterial morphologies were among those that were the most highly contrasting. The inclusions were ill defined, and the few reticulate bodies present were dispersed in the cytoplasm (Fig. S3).

In all, cell culture growth and phenotype assessments revealed that many Tn mutant strains displayed defects that represented significant differences from the parental strain. However, these defects were relatively subtle, with peak EB titers fluctuating by approximately with 1 log fold, and inclusion sizes were often within 10% to 15% of sizes seen with the parental strain, although the inclusions seen with the *ct015::Tn* mutant were over 30% smaller than the parental inclusions. The extreme exception to these trends was mutant *ct696::Tn*, with gross defects in EB production and in bacterial and inclusion morphologies. Moreover, there was little correlation between EB production titers and inclusion sizes, with the exception of the hypothetical *ct550* encoding gene, which displayed more and larger inclusions.

***In vivo* assessment of infectivity.** While the majority of the Tn mutants analyzed showed minimal morphologic or growth differences under *in vitro* cell culture conditions, some gene products may be of greater significance under the more physiologically relevant, diverse, and challenging conditions associated with mammalian infection. In order to assess this, a mouse model of *C. trachomatis* infection was implemented. Unfortunately, *C. trachomatis* L2 administered vaginally in mouse infections is readily cleared, rarely and unreliably ascends to the upper genital tract, and is not associated with the development of pathology (43, 44). As such, the transcervical model was used to deliver infectious doses directly into uterine horns of the upper genital tract (45). Previous experiments have shown that transcervical *C. trachomatis* infection of uterine horns typically peaked between 3 and 6 days postinfection and that the bacteria cleared (nearly 3 log-fold) after ~9 days postinfection (45). Therefore, to discover potential deficiencies in infection and replication in the upper genital tract, mice were infected with individual Tn mutants and harvested on day 5, within the period of the peak of *C. trachomatis* L2 infection.

Twelve Tn mutants that were evaluated for growth and morphology, including the parental strain and *ct383/4::Tn* clones, were used to infect mice and assess bacterial burden (Fig. 4). Most of the Tn mutants displayed infection levels similar to those seen with the parental *C. trachomatis* strain; however, two Tn mutant clones showed statistically significant decreases in levels of detectable organisms in the uterine horns compared to parental L2 ($P < 0.05$; Fig. 4). Disruptions in a FAD-dependent monooxygenase (FDM) (*ct148*) and the *cd1* deubiquitinase (*ct868*) were followed by a nearly 0.5 log-fold to 1 log-fold decrease in the levels of detectable organisms compared to the WT. Mutant *ct148::Tn* showed a striking deficiency with respect to detectable organisms, with 4 of 10 infected animals showing infection levels falling 2-log below the median of infection for WT-infected animals. Interestingly, mutant *ct148::Tn* displayed a slightly enhanced level of production of infectious progeny *in vitro* (Fig. 2C) relative to the parental strain. Conversely, mutant *ct868::Tn* showed no decreased growth rates *in vitro*, suggesting that *cd1* is dispensable for optimal growth in cell culture but that the absence of the corresponding gene product is important for growth *in vivo*. Importantly, the

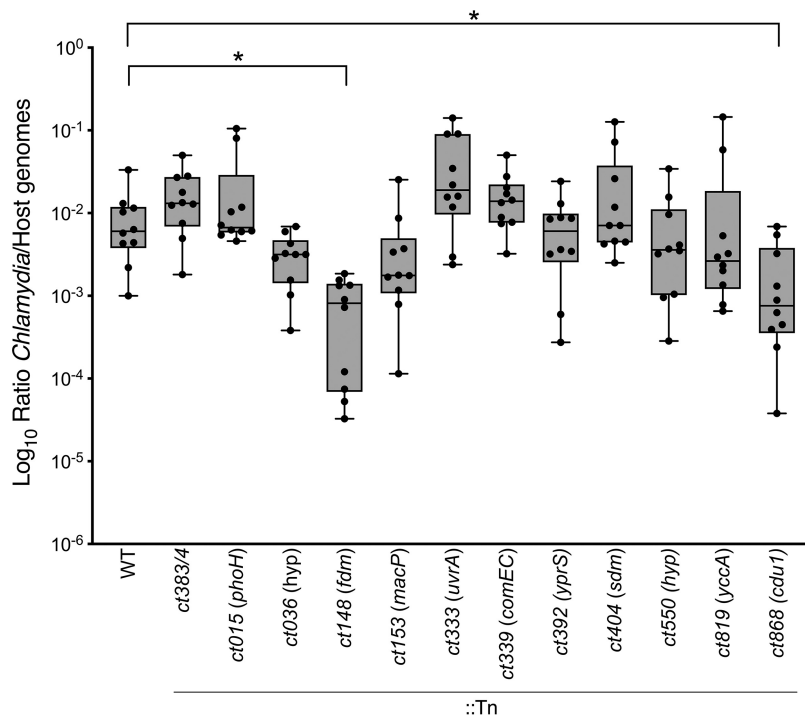


FIG 4 *In vivo* infections using Tn mutants with a trans cervical mouse infection model. Groups of 10 female C57BL/6 mice were infected trans cervicaly with 5×10^5 IFU of either parental (WT) *C. trachomatis* or Tn mutants as indicated. Five days postinfection, genital tracts were harvested and DNA was purified from uterine horns. Bacterial burdens were calculated as levels of *Chlamydia* genomes relative to host genomes, and ratios are shown as box-and-whisker scatter plots representing data from 10 mice. *, $P < 0.05$ (unpaired Student's *t* test).

bacterial burdens seen with *ct868::Tn* infections were very similar to the levels previously reported from a study performed with this mutant strain (46), providing additional confidence in the reproducibility of these observations. While the results were not statistically significant, two additional mutants exhibited a noticeable decrease in bacterial burden, namely, mutants *ct036::Tn* (hypothetical) and *ct153::Tn* (membrane attack complex/perforin [MACPF]). Mutant *ct036::Tn* was among the clones that displayed lower levels of progeny production whereas mutant *ct153::Tn* produced more infectious progeny than the parental clones.

Clearly, further temporal and spatial analyses in mice, detailed molecular and cellular studies, and genetic complementation are required for a more complete understanding of the role and function of gene products with demonstrated deficiencies in mice. However, these comparative *in vitro* and *in vivo* observations highlight that certain gene products may exhibit a more pronounced fitness defect in mice, prompting a focus on these gene products.

***In silico* analyses of CT339 support functional identification of CT339 as DNA uptake protein ComEC.** *Chlamydia* bacteria have been demonstrated to acquire and integrate DNA within or between certain *Chlamydia* species (24, 25, 47–49). Given the expected importance of lateral gene transfer in the evolution and adaptation of *Chlamydia*, as well as the paucity of identifiable gene candidates that may play a role in this fundamental process, the Tn insertion in *ct339* was of particular interest for a more in-depth analysis among the members of the subset of Tn mutants. CT339 shares similarity with multiple competence-associated protein families and conserved domains, including ComEC (E values ranging from $2.33e-03$ to $4.40e-24$). In both Gram-negative and Gram-positive bacteria, ComEC plays a key role as an inner membrane protein, transporting single-stranded DNA (ssDNA) into the cytosol of the bacterial cell during natural DNA acquisition (50, 51). To further investigate the hypothesis that *ct339* encodes a ComEC homolog, *in silico* analyses were performed.

ComEC is an integral membrane protein that typically has 9 to 12 transmembrane helices and a conserved metal-binding motif, HΦxxΦSGΦH ("Φ" indicates hydrophobic residues; Fig. S5A) (50). Topology modeling of CT339 using five hydropathy programs resulted in a range of 8 (SPLIT) to 11 (MEMSAT) predicted transmembrane segments, which is similar to the proposed 9 to 12 transmembrane regions of ComEC (50). As previously described for ComEC (50), HMMTOP prediction identified a large N-terminal loop within CT339 spanning residues 94 to 256 with a potentially stabilizing disulfide bond formed by C148-C167, as well as the competence domain containing the conserved metal-binding motif HΦxxΦSGΦH. For all five hydropathy programs, an extracellular N-terminal domain and intracellular C-terminal domain were predicted, similar to those of ComEC (50). In contrast to the predicted topology of ComEC, none of the predictive transmembrane helices for CT339 display an amphipathic character and no segments are predicted to be buried parallel to the membrane surface (Fig. S5B) (50). On the basis of these *in silico* data, a transmembrane topology model was designed (Fig. S5C) supporting the structural homology between CT339 and ComEC, specifically within conserved competence domains and the N-terminal loop. Using this model, the Tn insertion site was identified within the last transmembrane segment, eliminating G490 through the carboxyl end of the protein, L509. It has been proposed that ComEC from *Bacillus* exists as a homodimer within the bacterial membrane and forms a pore for DNA uptake (50). Consequently, disruption of either the N-terminal loop or the C-terminal loop, as is observed with *ct339::Tn* insertion, may prevent proper folding and formation of this pore, therefore abolishing the ability to acquire DNA.

Requirement of CT339 for DNA uptake via lateral gene transfer. As previously mentioned, the transposon insertion in *ct339* provided an opportunity to experimentally evaluate the importance of this gene product in lateral gene transfer and to support the *in silico* prediction of CT339 as a functional homolog to ComEC. Lateral gene transfer, including the transfer of specific antibiotic resistance genes, has been demonstrated to occur readily during coinfections with *C. trachomatis* strains (intraspecies) that encode different OmpA serotypes (25, 47). To evaluate the importance of CT339 in lateral gene transfer, intraspecies coinfections with different parental OmpA serovar strains (L1 or L2) encoding different antibiotic markers (L1 *tet^r* or L2 *bla*) under conditions of dual antibiotic selection were performed (Fig. 5A). Each L2 strain used had either an intact (*ct383/4::Tn bla*) or a disrupted (*ct339::Tn bla*) *ct339* gene. The relative levels of genetic transfer, particularly of the antibiotic marker, of the OmpA serovar strains were assessed by determining the quantity of progeny generated that exhibited each parental OmpA serotype (e.g., L1 versus L2).

Intraspecies coinfections and dual antibiotic selection with tetracycline-resistant *C. trachomatis* L1 (L1::*tet^r*) and either the transposon control mutant L2 *ct383/4::Tn bla* or the proposed ComEC homolog disrupted clone L2 *ct339::Tn bla* were performed (Fig. 5) (Table 3). When *C. trachomatis* L1::*tet^r* and L2 *ct383/4::Tn bla* were used for coinfections, high levels ($>6 \times 10^5$ IFUs) and nearly equal amounts of recombinant progeny displaying either parental OmpA (58% L1 and 42% L2) were observed. The relatively equal frequencies support the idea that DNA uptake and lateral transfer of the *tetR* gene from the L1 strain into to L2 genome occurred as efficiently as that of the *bla* gene from the L2 strains into the L1 strain. In contrast, when the same L1::*tet^r* parent was used in a coinfection with L2 *ct339::Tn bla*, similar levels of L1 OmpA-expressing progeny with dual resistance were detected (5.17×10^5 IFUs) but nearly 100-fold-lower levels of progeny displaying L2 OmpA were observed (7×10^3 IFUs) (Table 3). This supports the idea that DNA uptake and transfer of the *bla* gene into L1, which has an intact *ct339* gene, were as efficient as the previous cross. In contrast, *tetR* was found to be incorporated into the L2 genome with the *ct339::Tn bla* mutation at a 2 log-lower level. While this supports the idea of the importance of CT339 (*comEC*) in DNA acquisition, the low level of *tetR* resistance suggests that the *comEC* gene product may not be essential for the process.

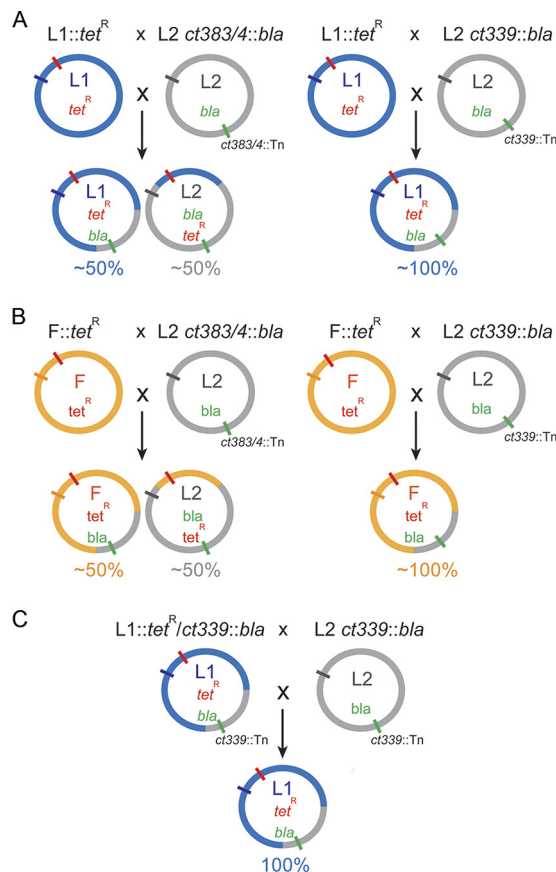


FIG 5 Graphic depiction of intraspecies recombination to evaluate functional role of CT339 in lateral gene transfer. (A) Parental *C. trachomatis* with L1 *ompA* (blue circle, blue tick) encoding *tet^r* (red tick) crossed with *C. trachomatis* with L2 *ompA* (gray circle, gray tick) containing either *ct383/4::Tn bla* (green tick) or *ct339::Tn bla* (green tick) to enable lateral gene transfer of resistance markers and selection of dual resistance chimeric clones (blue and gray circles). (B) Similar experiment using parental *C. trachomatis* with F *ompA* (yellow circle, yellow tick) encoding *tet^r* (red tick) crossed with *C. trachomatis* with L2 *ompA* (gray circle, gray tick) containing either *ct383/4::Tn bla* (green tick) or *ct339::Tn bla* (green tick). Serovar-specific antibodies revealed the relative distributions of resulting dually resistant chimera organisms (yellow and gray circles). Quantitative evaluations of resulting chimeras are provided in Table 3. The resulting mix of L1 (blue) and L2 (gray) or of F (yellow) and L2 (gray) reflects the almost equal amounts of resulting OmpA serovar seen when the control *ct383/4::Tn* was used. In contrast, virtually all of the resulting organisms contained a L1 (blue) or F (yellow) *ompA* when *ct339::Tn* was used, indicating that the *tet^r* gene, near *ompA*, was unable to be transferred into the L2 *ct339::Tn* mutant (gray). (C) Recombinants resulting from the experiment represented in panel A containing L1 *ompA* (blue circle, blue tick) encoding *tet^r* (red tick) and the *ct339::Tn bla* (green tick) were crossed with the L2 *ct339::Tn bla* mutants. All resulting progeny contained the L1 *ompA* (blue tick).

An alternative hypothesis to explain the low level of L2 OmpA-positive samples seen following the L1::tet^R and L2 *ct339::Tn bla* crosses is that, instead of poor uptake of the *tet^r* gene into L2 *ct339::Tn bla* organisms, a region of DNA that included the L2 *ompA* gene and the *ct339::Tn bla* marker was transferred and integrated into L1 parent organisms. This would “convert” the L1 to an L2 OmpA serotype. To investigate this hypothesis, whole-genome sequencing was performed on several individual recombinants from each coinfection (L1::tet^r versus L2 *ct339::Tn bla* or L2 *ct383/4::Tn bla*). As

TABLE 3 Frequency of *C. trachomatis* serotype (OmpA) following coinfection and dual antibiotic selection

<i>C. trachomatis</i> genotype	<i>C. trachomatis</i> serotype and frequency (%)		
L1::tet ^r × L2 <i>ct383/4::Tn bla</i>	L1 OmpA; 8.67 (±0.58) × 10 ⁵	L2 OmpA; 6.33 (±0.58) × 10 ⁵	L2 OmpA progeny; 42.2 (±1.99)
L1::tet ^r × L2 <i>ct339::Tn bla</i>	L1 OmpA; 5.17 (±0.43) × 10 ⁵	L2 OmpA; 7.00 (±1.00) × 10 ³	L2 OmpA progeny; 1.12 (±0.40)
F::tet ^r × L2 <i>ct383/4::Tn bla</i>	F OmpA; 4.33 (±1.15) × 10 ⁵	L2 OmpA; 3.33 (±0.58) × 10 ⁵	L2 OmpA progeny; 44.0 (±6.26)
F::tet ^r × L2 <i>ct339::Tn bla</i>	F OmpA; 1.33 (±0.61) × 10 ⁴	L2 OmpA; 5.33 × 10 ⁰ (±1.53)	L2 OmpA progeny; 0.05 (±0.01)

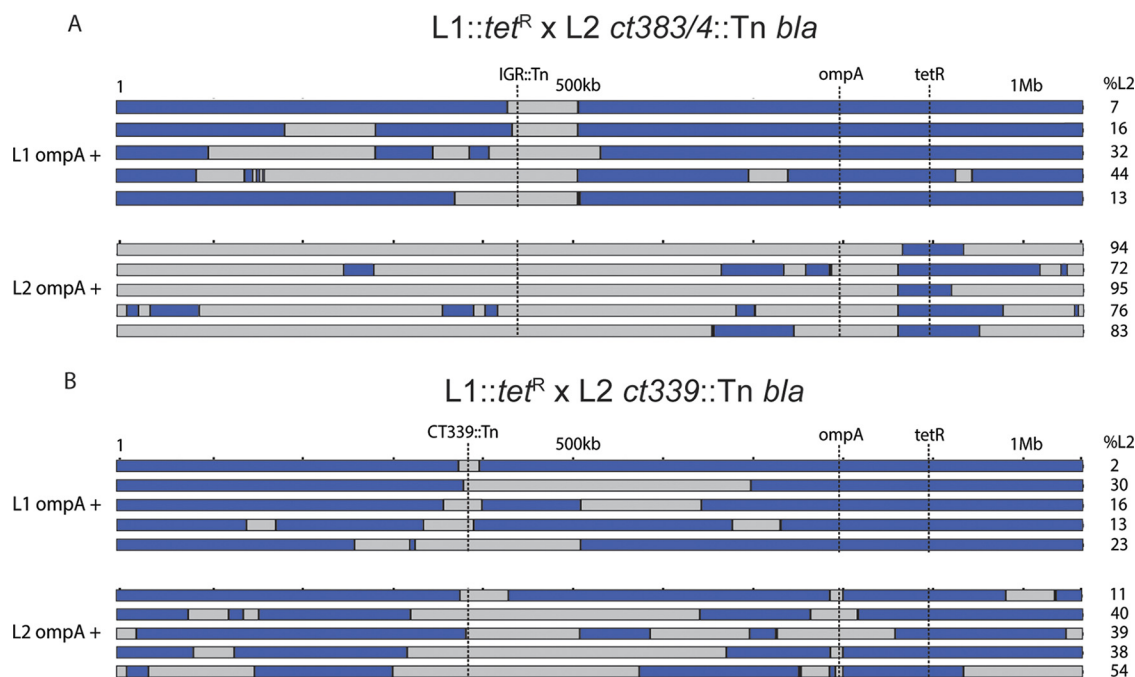


FIG 6 Schematic representation of regions and genome compositions of *C. trachomatis* recombinant clones following lateral gene transfer with selected Tn mutants. Blue bars represent the regions of the genome from the L1/*tet^R* parent. Gray bars represent regions from either L2 *ct383/4*::Tn *bla* or L2 *ct339*::Tn *bla* parent. Percentages of the *C. trachomatis* L2 genome present are indicated (right). (A) Progeny genomes from crosses between tetracycline-resistant *C. trachomatis* L1 and *ct383/4*::Tn *bla*. (B) Progeny genomes from crosses between tetracycline-resistant *C. trachomatis* L1 and *ct339*::Tn *bla*.

indicated in Fig. 6A, L1::tet^R and L2 *ct383/4*::Tn *bla* crosses yielded genomes that predominantly reflected the OmpA serotype (mostly blue for L1 OmpA and mostly gray for L2 OmpA). Specifically, L1 or L2 OmpA-positive samples had an average of 78% L1 or 84% L2 genomic composition, respectively. In contrast, L2 OmpA-positive samples generated after a L1::tet^R × L2 *ct339*::Tn *bla* coinfection had minimal L2 genome in the resulting clones (L2 [gray]; Fig. 6B), with an average genomic L2 composition of 36%, representing less than half the level observed in L1::tet^R × L2 *ct383/4*::Tn *bla* crosses. Matching the levels of antibiotic resistance transfer in *ct339* intact samples (L2 *ct383/4*::Tn *bla*), L1 positive OmpA samples showed an average of 80% L1 genomic composition (blue; Fig. 6B). These data support the hypothesis that DNA regions containing an L2 *ompA* gene and the *ct339*::Tn *bla* marker were most likely acquired by L1 parent clones through lateral gene transfer instead of *tetR* acquisition of a L2 *ompA ct339*::Tn *bla* organism.

The generation of L1::tet^R/*ct339*::Tn *bla* recombinant clones provided an additional opportunity to further investigate the essentiality of *ct339* for DNA acquisition and genome incorporation. These clones were used in coinfections with the parent L2 *ct339*::Tn *bla* clone with dual antibiotic selection (Fig. 5C). If *ct339* were essential for DNA acquisition and incorporation, then all resulting clones should be only L1 OmpA positive, as the L2 *ompA* gene would not have the ability to be transferred and incorporated into the L1 genome to enable a serotype conversion. However, if *ct339* is only partially required, then a mix of L1 and L2 OmpA populations would be expected to be observed following coinfection and antibiotic selection (i.e., with the *tetR* marker taken up and incorporated into the L2 genome or L2 OmpA transferred and incorporated into the L1 genome). Three independent coinfections revealed that only L1 OmpA-positive inclusions were observed with extensive (~5 × 10⁷) levels of IFUs utilized per evaluated cross (data not shown). Additionally, transformation of the L2 *ct339*::Tn *bla* mutant was also attempted using an inducible green fluorescent protein (GFP) plasmid (pTLR2-GFP) and chloramphenicol for selection. Every attempt to trans-

form parental L2 samples that had an intact chromosomal *ct339* gene was successful using the inducible plasmid. In contrast, none of the attempts to transform L2 *ct339::Tn bla* with the plasmid were successful (data not shown).

To further address the functionality of CT339 in lateral gene transfer, similar coinfections and dual-selection experiments were performed with tetracycline-resistant *C. trachomatis* serovar F (F::*tet^r*). Using strains that are more phylogenetically distant (52) reduces the challenge of delineating highly similar genomic crossover regions. Three independent crosses and selections were performed with *C. trachomatis* F::*tet^r* and either *C. trachomatis* L2 *ct383/4::Tn bla* or *C. trachomatis* L2 *ct339::Tn bla* (Fig. 6B). As observed in the L1 × L2 *ct383/4::Tn bla* experiments (Fig. 6A) (Table 3), approximately half of the inclusions with an intact *ct339* exhibited either OmpA F (56%) or L2 (44%) seroreactivity (Table 3). Similarly to the L1::*tet^r* versus L2 *ct339::Tn* crosses, more than 99.94% of the F::*tet^r* × L2 *ct339::Tn* inclusions were positive for only OmpA F (Table 3). Taken together, these data support the hypothesis that *ct339* is critical for DNA uptake and is likely serving as a ComEC functional homolog in *C. trachomatis*.

DISCUSSION

There have been many recent firsts in the area of genetically modifying *Chlamydia trachomatis*, including chemical mutagenesis (35–37), group II intron gene disruption systems (29), allele replacement (33, 34, 53), inducible gene expression (28, 54), and targeted gene repression (32). The development and validation of a transposon mutagenesis system using the *Himar1* transposase, as presented here, provide another first and a key advance for the *Chlamydia* field. The data presented demonstrate that the transposase is functional within *Chlamydia* and that the use of the nonreplicative plasmid results in mutant *C. trachomatis* clones containing a single genomic insertion. The insertion sites are readily discovered and can be characterized by common PCR-sequencing-based techniques. These insertion mutations are stable, even without antibiotic selection, limiting the chances of genetic reversion. Support for this stability was provided by the multiple passages and large-scale growth conditions (3 to 5 passages for expansion and spinner flask cultivation), without antibiotics, employed prior to animal studies as well as by the confirmation of Tn insertions in samples prior to and after animal infections. A primary benefit of this single-insertion, random mutagenesis approach is the ability to associate a specific genetic disruption with a resulting phenotype. While polar effects can occur as the result of a Tn insertion, such effects can be viewed as a benefit, as an insertion can enable researchers to focus on a selected but known pool of candidates associated with a particular phenotype. As demonstrated by the insertion disruption of ComEC homolog CT339 and by the subsequent biological studies related to lateral gene transfer in *Chlamydia* presented here, the scientific contributions of this molecular tool and approach are expected to be very useful for *Chlamydia* studies.

Notwithstanding these benefits, the present report also highlights the relatively low efficiency associated with *Chlamydia* transposon mutagenesis and its current limitations for large-scale studies. While most of this restriction is thought to be due to the extremely poor transformation efficiency associated with *C. trachomatis*, the low insertional efficiency may also suggest that high numbers of genes are essential for growth and completion of the chlamydial developmental cycle under cell culture conditions. A total of 70 genes incurred a Tn insertion in this study, while the results of a random chemical mutagenesis study performed by Nguyen and Valdivia (37) indicated that 84 protein-coding genes incurred a nonsense mutation with limited *in vitro* growth effects. Fifteen of the 84 genes were also disrupted in that Tn insertion analysis, providing a total of 139 genes that have disruptions in the coding region following ethyl methanesulfonate (EMS) mutagenesis or Tn insertion. This represents around 15% of the encoding gene products. While the number of genes that are essential for growth under tissue culture conditions is currently unknown, the relative low level of overlap of disruptive Tn and EMS mutations suggests that many more *C. trachomatis* genes may tolerate disruption.

Among the more striking observations were the enhanced *in vitro* growth of a *ct148::Tn* mutant clone and the almost log-fold decreased infectivity in mice (Fig. 2C; see also Fig. 4). The Tn insertion occurs in the first third of the coding region, providing higher expectations that the function of this gene product is indeed disrupted. The gene downstream from *ct148* is oriented in the opposite direction, although there is a gene 200 bp upstream. This distance and the reported location of the transcriptional start site 85 bp upstream of *ct148* (40) support the idea that there is a single gene operon and that polar effects from this Tn insertion are limited. The *ct148* gene encodes a FAD-dependent monooxygenase (FDM). Monooxygenases are known to play roles in multiple metabolic pathways, and, as Iliffe-Lee and McClarty showed previously (55), *C. trachomatis* contains an almost complete and functional Embden-Meyerhof glycolysis and pentose phosphate pathway. For a number of other bacteria, it has been shown that metabolic proteins are nonessential for growth *in vitro* and yet play vital roles *in vivo* (8, 56–58). Many of the key nutrients required for survival are provided in media used to grow these pathogens. Thus, any detrimental effect that a mutation may have may not be as easily identified *in vitro*. In contrast, *in vivo* infections provide physiological conditions for growth which are not provided via media, enabling the effects of these mutations to be detected. While the specific role of *ct148* in infectivity remains unknown, the *in vivo* data provide support for the idea that components that are seemingly nonessential for *Chlamydia* growth in tissue culture may, in fact, play significant roles in mammalian models of infection. A similar discrepancy between *in vitro* and *in vivo* growth outcomes was also observed with the *ct868::Tn* clone which disrupts *cd1*. Cdu1 is a deubiquitinase, and it has been shown that disruption of this protein results in an increase of ubiquitination of Mcl-1 (46). Cdu1 has also been demonstrated to be capable of inhibiting host NF- κ B, which represents a central regulator of numerous immune responses, including cytokine secretion and T-cell proliferation, and a vital host defense against intracellular pathogens (59–61). Overall, these observations highlight the challenges and potential discrepancies of functional studies performed in tissue culture, strengthening the necessity for analysis using *in vivo* models of infection.

The most striking phenotype was that of the observable growth and morphological deficiencies of strain *ct696::Tn* (see Fig. S2 in the supplemental material). First classified as a slow grower, approximately 8 days of growth of *ct696::Tn* were required for detection of visible inclusions by phase microscopy, and subsequent analysis by confocal microscopy identified decreased numbers of RBs/EBs as well as the absence of the nuclear localization typically observed with *Chlamydia* inclusions. Due to its genetic location near the genes encoding the known type III secretion (T3S) effector proteins CT694 and CT695, it has been hypothesized that *ct696* may also play a role in T3S; however, studies have suggested that this may not be the case. Secretion of CT696 was not observed in previous studies employing a heterologous T3S system with *Yersinia enterocolitica* (62, 63), and *ct696* transcription was found to occur independently of *ct694* (64, 65). The *ct696* gene (*ctI0065*) was also disrupted using allelic exchange (33); however, growth phenotypes were not provided. CT696 is a conserved *Chlamydiaceae* hypothetical protein with no sequence or conserved domains shared outside the members of this family. Using the bacterial localization tool PSORTb (66), CT696 was predicted to be a cytosolic protein. While additional in-depth analysis is required to evaluate the role and function of CT696 in growth and inclusion formation, this observation provides support for these efforts as well as a good example of the utility of this transposon approach for discovery of genes important to the biology of *Chlamydia*.

Along with gaps in understanding the mechanisms of development and *in vivo* infectivity of *Chlamydia*, there is also limited information regarding the components and mechanisms for lateral gene transfer. The absence of lateral gene transfer in organisms that contain the *ct339::Tn* insertion provides compelling support for the essential contribution of this gene product to this fundamental evolutionary process. CT339 is predicted to be a multipass transmembrane protein with domain similarity to

ComEC, the competence uptake protein seen in many bacteria. According to the protein family database (pfam) architecture, genes encoding proteins with this competence motif often exist near genes encoding proteins that include lactamase-superfamily domains, which are predicted to regulate the competence operon (67). Baker et al. recently showed the ComEC from *Bacillus* contains a β -lactamase-like domain within its C-terminal loop (approximately residues 494 to 763), potentially functioning as a nuclease (68). While it is widely accepted that double-stranded DNA (dsDNA) must first be converted into ssDNA for uptake and incorporation into recipient genomes, the nuclease responsible for this activity in *Bacillus* remains unknown; thus, it has been hypothesized that this lactamase-like domain within ComEC may be fulfilling this role. As a potential homolog of ComEC, a Tn disruption in the C terminus of CT339 may prevent the degradation of dsDNA into ssDNA and would decrease the ability of *Chlamydia* to undergo lateral gene transfer. However, Pfam and SMART (69) analyses of CT339 did not identify a similar lactamase-like domain near the C terminus. Rather, genome analysis of *C. trachomatis* identified RNase Z (CT346), a lactamase-superfamily protein neighboring CT339—suggesting that this protein may instead be fulfilling that role in the chlamydial competence system. Future studies assessing the dimerization and pore formation of CT339 and potential nuclease activity of CT346 will assist in identifying how CT339 enables DNA uptake.

Other potential components involved in DNA uptake in *Chlamydia* are less evident. Pili or pseudopili predominantly facilitate binding and transport of DNA to the bacterial surface, although no proteins sharing any sequence similarity to pilus homologs were identified in *Chlamydia*. Interestingly, *Helicobacter pylori* is unique among naturally transformable bacteria in that it does not use pili but instead relies on a dedicated type IV secretion system for DNA uptake (70). Gram-negative bacteria typically transport dsDNA through an outer membrane secretin channel (e.g., PilQ) and then process the dsDNA into ssDNA with a periplasmic protein, ComEA. Single-stranded DNA is then transported through inner membrane protein ComEC and into the bacterial cytoplasm, where it is bound by RecA or DprA (71). Direct pairwise BLAST analysis of *C. trachomatis* with numerous Gram-negative secretin homologs (PilQ) revealed sequence similarity (E values $<10^{-9}$) to only type II and type III secretion outer membrane proteins, GspD (CT572) and YscC (CT674), respectively. Similarly, no protein with similarity to various ComEA or DprA homologs was identified through sequence-based pairwise analysis. Clearly, there is much to be learned about the *Chlamydia* DNA uptake system, although it is safe to state that, similarly to *H. pylori*, *Chlamydia* is likely an exception to the general DNA uptake model.

In summary, the development and characterization of a transposon system that is functional in *Chlamydia* represent a substantial advance and a valued addition to the growing repertoire of genetic manipulations in this field. Such a transposon system is expected to have an enabling effect on the discovery of biological and pathogenesis-related genes, allowing the association of single-gene insertions with evaluated phenotypes. Only a subset of the initial Tn insertion mutant clones was evaluated for *in vitro* and *in vivo* growth and infectivity. An expanded analysis of the remainder of the Tn insertional clones by the use of these and other phenotypic screens will elucidate the contribution and role of various gene products. This report has also highlighted the current inefficiency in transformation in *Chlamydia*, which will need to be overcome for large-scale mutagenesis studies. Despite this shortcoming, there is much promise for this technique and its associated applications, as evident from the support for CT339 in the fundamental evolutionary process of lateral gene transfer in *Chlamydia*. There are also high expectations that this system will be applicable and functional for studies in other *Chlamydia* species and serovars (e.g., *C. muridarum* and *C. trachomatis* serovar D), thus enabling animal studies and analysis of more clinically relevant strains for the discovery of virulence factors and potential therapeutic targets.

MATERIALS AND METHODS

Chlamydial strains and propagation. *C. trachomatis* serovar L2 434/Bu was propagated in L929 mouse fibroblast cells (ATCC CCL-1) using RPMI 1640 medium (Invitrogen, Grand Island, NY) supplemented with 5% heat-inactivated fetal bovine serum (FBS) plus 10 $\mu\text{g/ml}$ gentamicin (Fisher Scientific, Pittsburgh, PA). Briefly, L929 monolayers were grown to confluence in spinner flasks ($\sim 8 \times 10^5$ cells/ml) and infected with purified EBs at a multiplicity of infection (MOI) of 1. Cultures were allowed to grow for up to 48 h at 37°C and 5% CO_2 . Percent infectivity was assayed by IFA microscopy (described below). EBs were harvested as previously described (72) using a series of centrifugation and sonication steps to disrupt the host cells and release EBs. Once isolated, EBs were either frozen immediately or further purified using Omnipaque (Barrington, IL) and ultracentrifugation. All EBs were stored in sucrose-phosphate-glutamic acid (SPG) media at -80°C . Clonal isolates were obtained as previously described (73).

Development of pCMA transformation plasmid. pUC19 (GenBank accession no. [L09137](#)) was used as the initial backbone for pCMA generation and primers used are listed in Table S1 in the supplemental material. The C9 hyperactive transposase was amplified from pBADC9 (kind gift from D. Lampe of Duquesne University [3]) and cloned between the EcoRI and AatII sites. An EagI site was incorporated for subsequent promoter cloning. Initially, a vector (pCMT) that contained a tetracycline-encoding transposon was generated for application in *C. muridarum* by the use of pACYC184 (GenBank accession no. [X06403](#)) as the template. Primers incorporated *Himar* inverted repeats and restriction sites for cloning into the XmaI site. To remove the β -lactamase gene carried on pUC19, the transposase, tetracycline transposon, and *ori* region were amplified with primers containing NcoI sites for self-ligation. Ligase-independent cloning and HindIII sites were used to replace the tetracycline transposon with one encoding the β -lactamase and the associated promoter from pSW2 (27). To assist with selective expression of the transposase within *Chlamydia* and with less expression during plasmid propagation in *E. coli*, the chlamydial *ct559* promoter and ribosomal binding sites were cloned upstream of the transposase gene using the EagI site (38). The complete DNA sequence for pCMA is provided in the supplemental material. The graphical depiction of the plasmid (see Fig. S1 in the supplemental material) was generated using Savvy Scalable vector graphics (74).

Transposon mutagenesis. The method used for transformation of *C. trachomatis* was modified from previously described methods (27, 39). L929 cells were seeded to confluence in 6-, 12-, or 24-well plates and allowed to adhere overnight. The *Chlamydia*-DNA transformation reaction mixture (200 μl total volume) was prepared with 10 μl of *C. trachomatis* L2 434/Bu EB seed stock, $1 \times$ SPG ($\sim 1 \times 10^7$ IFU), 15 μg of pCMA plasmid DNA, and 100 μl of $2 \times$ CaCl_2 buffer (20 mM Tris-HCl [pH 7.5], 100 mM CaCl_2), with double-distilled water (ddH_2O) added to reach the final volume. Following gentle pipette mixing, the reaction mixtures were incubated for 30 min at room temperature (RT). The mixture was added to 12 ml of $1 \times$ CaCl_2 buffer (10 mM Tris-HCl [pH 7.5], 50 mM CaCl_2) before being overlaid onto a L929 monolayer that was washed once with $1 \times$ CaCl_2 buffer (10 mM Tris-HCl [pH 7.5], 50 mM CaCl_2). Plates were spun at $550 \times g$ for 30 min at RT. Fresh RPMI medium supplemented with FBS, gentamicin, and 1 $\mu\text{g/ml}$ cycloheximide was added, and the plates were incubated at 37°C and 5% CO_2 overnight. Ampicillin (Fisher Scientific, Pittsburgh, PA) (1 $\mu\text{g/ml}$) was then added for antibiotic selection at 16 to 18 h postinfection. Cultures were kept under conditions of selection using increasing concentrations of antibiotics and serially passaged every 48 hpi. After the final passage, EBs were harvested for identification of insertion site and subsequent analyses. Transformation efficiencies were estimated using 1×10^7 IFU input organism and 15 μg plasmid DNA, resulting in an average of 4 unique clonal isolates from each transformation (4 IFU/15 μg DNA). Twenty-three transformations were performed, resulting in 105 ampicillin-resistant cultures. The levels of transformation efficiency were separately assessed with five independent transformations using pGFP::SW2 plasmid under similar conditions and the same stocks of *C. trachomatis* as were used in transposon mutagenesis.

Whole-genome sequencing. DNA was extracted from purified EBs using a Qiagen blood and tissue kit (Qiagen, Valencia, CA). Manufacturer's instructions were used with minor modifications. In brief, purified EBs were aliquoted with buffer AL before proteinase K was added and the reaction mixtures were incubated at 56°C for 1 h. After incubation, buffer AL and ethanol (96% to 100%) were added and mixed thoroughly by the use of a vortexing mixer. The reaction mixtures were added onto a provided DNeasy Mini spin column and collection tube and were centrifuged at $6,000 \times g$. Two wash steps were then performed using buffer AW1 and AW2, each with centrifugation. Finally, the reaction mixtures were incubated with buffer AE for 20 min at room temperature and centrifuged and the eluate was saved. For quality control, each sample was verified using a spectrophotometer (Denovix Ds-11 FX+) to quantify DNA. Extracted DNA was prepared for sequencing at the Genome Sequencing Core at the University of Kansas, where library preparation and further quality control were completed. Samples were multiplexed and run on an Illumina Miseq PE100 platform. Paired-end reads were generated with a Phred score ($>Q30$) of 95.44%. Reads were then demultiplexed and analyzed using the Geneious software suite. Total read coverage was calculated as a function of the proportion of reads that mapped to the WT reference genome (the total of chlamydial reads) over the total number of reads generated for the sample, including host DNA and other contaminant DNA. A threshold of 10 reads was created to check for the depth of coverage at each base pair (75).

Assembly and analysis of the transposon mutant genomes. The *C. trachomatis* LGV 434/Bu ("Hefty") parental clone sequence (NCBI sequence accession no. [CP019386.1](#)) was generated through assembly guided by reference to the previously published genome *Chlamydia trachomatis* 434/Bu (NCBI sequence accession no. [NC_010287.1](#)). The Hefty parental genome sequence contained three mutations relative to the reference strain, namely, two nonsynonymous mutations (G946945A [H1121N] and

C942546A [R274H]) and one intergenic indel (indel in lowercase; 127353/4 [AGGCCattctaaagccCC CTT]). After the parental draft was generated, each of the other samples were generated using the parental sequence as the reference sequence. In each case, read depth and potential loss of read continuity were considered for potential duplications or rearrangements. The reads were also mapped to the transposon sequence for each sample to ensure that the transposon was inserted into the correct site at the genome. Alignment files were generated for alignments between each mutant genome draft and the parental draft. Any mutations corresponding to these that might have accumulated through the study were annotated and verified using the reads. Host DNA contamination within each sample was mitigated using the reference-guided assembly techniques. Transposon insertion sites were analyzed both through the use of the reference-guided mapping of the genomes and separately through the use of reference-guided assembly of the raw reads to the transposon sequence. In each case, these were analyzed separately from the hypothesized insertion sites to prevent bias. The read quality of the transposon assemblies was proportional to the size of each genome in every case. Plasmid sequences were generated for each sample by using the *C. trachomatis* LGV plasmid (NCBI sequence accession no. [NC_021051.1](#)). Plasmid gene assignments incorporated both *pgp1-8* (42) and *cds1-8* (76) nomenclature. All alignments were performed in Geneious using global alignment with free end gaps and a cost matrix corresponding to 65% similarity. Completed sequences were submitted to GenBank and assigned accession numbers (see "Data accessibility" section below). The transposon mutant genomes were evaluated for new single nucleotide polymorphisms (SNPs), and no mutations were discovered after the transformation and cultivation processes. While all studies were performed using *C. trachomatis* LGV 434/Bu, *C. trachomatis* serovar D gene nomenclature is utilized due to recognition and field familiarity.

Assembly and analysis of the recombinant progeny genomes. Each recombinant genome was generated using assembly guided by reference to the OmpA parental genome. Genomes were then aligned to both parental genomes and scanned for regions of homology using the Geneious global alignment tool with free end gaps and a cost matrix corresponding to 65% similarity. Initial sequence assembly was verified through assembly guided by reference to the minority parent. Regions of homology were annotated, and margins were estimated based on similarity to the individual parents.

In vitro growth analysis of Tn mutants. For temporal assessment of progeny production, L929 mouse fibroblast cells were infected in triplicate with *C. trachomatis* parental or Tn mutant clones with a multiplicity of infection (MOI) of 0.5 in 24-well plates. At 18, 24, 30, 36, and 42 h postinfection (hpi), wells were washed once with Hanks' balanced salt solution (HBSS) and then immediately frozen in 1× SPG at −80°C within the 24-well plate. The 24-well plates were then thawed on ice and transferred to 1.5-ml Eppendorf tubes and sonicated in a Q500 Qsonica cuphorn sonicator (Qsonica) with the following settings: 75% amplitude; 4 pulses; 30-s ON/30-s OFF cycle in chilled (~5°C) water. To determine titers of inclusion-forming units, samples were then serially diluted and used to infect confluent monolayers of L929 mouse fibroblast cells in 96-well μ Clear CellStar plates (catalog no. 655090; Greiner Bio-One, Frickenhausen, Germany) or 8-well μ -Slides (Ibidi, Martinsried, Germany). After 24 h postinfection, the cells were washed with HBSS and then fixed with 100% methanol. Cells were washed with phenol-free HBSS before staining was performed with a MicroTrak *C. trachomatis* culture confirmation kit (Trinity Biotech, Wicklow, Ireland). After at least 1 h of room temperature incubation, 1 μ M DAPI (4',6-diamidino-2-phenylindole) diluted in phosphate-buffered saline (PBS) was added and allowed to stain wells for 10 min. A final overlay of 0.1 M Tris-glycerol was added, and cells were imaged on an Olympus IX71 inverted microscope (Olympus, Waltham, MA) with both 10× and 40× objectives. Inclusions were enumerated manually for each sample by immunofluorescence microscopy. For calculation of progeny production, titers were also determined for the inoculum that was initially used to infect the 24-well plates at the time of infection to incorporate subtle differences in starting infectivity for each mutant relative to the parental strain (see Fig. S4 in the supplemental material). To normalize variations in Tn mutant progeny production that would result from differences in starting infectivity levels, the ratio of starting inoculum of the parental strain to the starting inoculum of the Tn mutant was individually multiplied by each Tn mutant's titers at each time point (18, 24, 30, 36, or 42 hpi). Data are shown as means and standard deviations (SD) for triplicate wells, generated in GraphPad Prism 7, and statistical differences were calculated using the two-tailed Student's *t* test. With a *P* value of <0.05, *ct732::Tn* had significantly reduced progeny production at 24, 30, 36, and 42 hpi; *ct590::Tn* and *ct036::Tn* had significantly reduced progeny production at 24, 30, and 42 hpi; *ct350::Tn* had significantly reduced progeny production at 30 and 42 hpi; *ct153::Tn* and *ct550::Tn* had increased progeny production at 24 hpi; *ct339::Tn* had increased progeny production at 24 and 42 hpi; and *ct148::Tn* had increased progeny production at 30 and 42 hpi.

Confocal immunofluorescence microscopy. L929 cells were grown to confluence in an 8-well ibiTreat μ -Slide (Ibidi, Martinsried, Germany) and were infected with the respective *C. trachomatis*/Tn mutants. At ~24 hpi, infected cells were fixed with 100% methanol for 10 min at RT. Cells were washed once with HBSS and again with PBS and then stained using the preparation supplied in the MicroTrak *C. trachomatis* culture confirmation test (Syva Co., Palo Alto, CA) (180 μ l) diluted 1:40 in PBS for 1 h 50 min at RT in the dark or overnight at 4°C. A 2- μ l volume of 1 μ M DAPI (4',6-diamidino-2-phenylindole) diluted 1:100 in PBS was then added to wells and allowed to stain for 10 min at RT in the dark. The stain was then removed, and the cells were washed with PBS. A final overlay of Vectashield antifade mounting medium (Burlingame, CA) was added, and slides were stored at 4°C in the dark until the imaging step. Cells were visualized on an Olympus IX81/31 spinning disk confocal inverted microscope at ×150 magnification and captured on an Andor Zyla 4.2 scientific complementary metal oxide semiconductor (sCMOS) camera (Belfast, Northern Ireland). Microscope and camera were operated using SlideBook 6 software (Intelligent Imaging Innovations, Denver, USA). Exposure time remained consistent for all fields captured, with the exposure time for DAPI set at 2 s, for OmpA at 4 s, and for cytoplasm at 6 s. Three to

seven Z stack images were taken at 0.3- μm intervals per cell imaged. Images were processed in SlideBook 6, and No Neighbors deconvolution (with a subtraction constant of 0.4) was applied to all images.

In vitro inclusion size analysis for Tn mutants. L929 mouse fibroblast cells were infected at low MOI (~10% of cells infected) in triplicate on two separate 96-well plates with parental population or a clonal population of Tn mutant *Chlamydia trachomatis*. At 24 hpi, cells were fixed with methanol for 10 min. Cells were then stained using a MicroTrak *C. trachomatis* culture confirmation kit for 1 h at room temperature. DAPI (4',6-diamidino-2-phenylindole) (1 μM) was diluted in PBS and allowed to stain wells for 10 min. A final overlay of 0.1 M Tris-glycerol was added, and cells were imaged on an EVOS FL Auto 2 microscope (Thermo Scientific, Waltham, MA) using a 20 \times objective. A total of 16 fields were imaged for 6 wells for each sample, including more than 200 inclusions per sample (range, approximately 200 to 1,000). Each inclusion area was then measured using MIPAR (MIPAR, Worthington, OH). Within MIPAR, segmentation of inclusions was performed by applying a threshold to images to identify inclusions based on a range of pixel values that was standardized to parental images. After segmentation of inclusions, the total area was measured and quantified as the total number of pixels. This output was then exported to GraphPad, and statistical analysis was performed. Statistical analysis consisted of a one-way analysis of variance (ANOVA) with Dunnett's multiple-comparison test (statistical significance *P* value, <0.05).

Mouse transcervical infections. Female C57BL/6 mice (6 to 8 weeks old) were purchased from Jackson Laboratories and housed in accordance with the requirements specified by the University of Kansas Institutional Care and Use Committee. Mice were treated subcutaneously with 2.5 mg medroxyprogesterone acetate (Depo-Provera, Pfizer, NY) upon arrival (day -7). Fresh aliquots of parental or Tn mutant *C. trachomatis* clones were diluted in sucrose-phosphate-glutamic acid (SPG) buffer and kept on ice until use. Using a nonsurgical embryo transfer device (NSET; ParaTechs, Lexington, KY), mice were inoculated transcervically with 10 μl diluted stock (final concentration, 5×10^5 IFU/mouse) by insertion of the device into the genital tract beyond the opening of the cervix. For each infection, samples used to infect mice were also evaluated for titer to ensure delivery of the expected infectious dose. The infections and analyses performed with *ct868::Tn* were repeated from the initially reported experiments (46).

ddPCR assessment of *Chlamydia* infection in vivo. Mice were humanely euthanized 5 days postinfection, and the genital tracts were collected in SPG. Uterine horns were homogenized using a rotor/stator homogenizer (Biospec, Bartlesville, OK). Aliquots (100 μl) were frozen at -20°C until use. The remaining stocks of homogenized tissues were stored at -80°C . DNA isolation was performed using the 100- μl aliquots and a DNeasy blood and tissue kit (Qiagen). Isolated DNA was then used for droplet digital PCR (ddPCR) analyses. Primers and probes for *C. trachomatis secY* and murine *rpp30* (see Table S1 in the supplemental material) were used with ddPCR Supermix for Probes (Bio-Rad, Hercules, CA) to set up the PCRs. Oil-for-Probes droplet emulsions were generated using a droplet generator cassette (Bio-Rad). The PCR conditions were as follows: 95°C for 10 min and 40 cycles of 94°C for 30 s and 98°C for 10 min followed by cooling to 4°C . Fluorescent reads of individual droplets were calculated after PCR was performed using a QX200 droplet reader (Bio-Rad). Data were analyzed using QuantaSoft Software (Bio-Rad), and the results are reported as \log_{10} ratios of *Chlamydia* DNA to host DNA (*secY/rpp30* copies/ μl). Box and whisker scatter plots were generated in GraphPad Prism 7, and recoverable organisms were compared using unpaired multiple *t* tests with no correction for multiple comparisons.

Bioinformatic analysis of CT339 and chlamydial competence. BLAST analyses and subsequent queries within the Conserved Domain Database resulted in hits within the competence superfamily and multidomain hits for ComEC. Multiple-sequence alignments were generated using ClustalW and 10 variable species hits within the Clusters of Orthologous Groups of proteins (COG0658) (77). The following proteins were used (NCBI accession numbers shown in parentheses): competence protein ComEC family protein *Shigella dysenteriae* 1617 (YP008850592.1), competence locus E *Helicobacter pylori* Hp P-26 (EJC51989.1); competence protein ComEC *Enterococcus faecium* DO (YP006375852.1); ComE *Synechocystis* sp. PCC 6803 (BAA17126.1); ComEC *Listeria monocytogenes* EGD-e (CAC99560.1); ComE operon protein 3 *Bacillus subtilis* subsp. *subtilis* strain 168 (NP 390435.1); hypothetical protein AGR C 2573 *Agrobacterium tumefaciens* sp. strain C58 (NP354400.1); competence protein *Neisseria meningitidis* MC58 (NP273744.1); hypothetical protein CT339 *Chlamydia trachomatis* D/UW-3/CX (NP 219846.1); ComEC/Rec2 family protein *Clostridium botulinum* A strain ATCC 3502 (YP 001255462.1); ComEA *Neisseria meningitidis* (CAB44958); ComEA protein *Helicobacter bilis* (WP_004084273); competence ComEA *Shigella dysenteriae* 1617 (EFP70107); competence protein ComGA *Enterococcus faecium* (WP_002304768); competence protein ComGA *Listeria monocytogenes* (WP_009933475); ComGA *Bacillus subtilis* (BAA12533); (multispecies) competence protein ComGB (WP_002286180); (multispecies) competence protein ComGB *Bacillus* (WP_048681721); competence protein ComGB *Listeria monocytogenes* (WP_010990101). (multispecies) type IV pilus secretin PilQ *Neisseria* (WP_016686778); type 4 pilus secretin PilQ (outer membrane porin) *Shigella dysenteriae* 1617 (AHA67697); (multispecies) pilus assembly protein PilE *Neisseria* (WP_002214937); and ComGC *Bacillus subtilis* (BAA12535). The following five hydropathy prediction programs were used to predict topology for CT339: HMMTOP v2.0 (78); MEMSAT-SVM (79); TMHMM2.0 (80); TOPPRED (81); and SPLIT (82). Transmembrane illustrations were generated and modified using Protter v1.0 (83).

Generation of recombinant clones for assessment of bacterial competence. All experiments performed with tetracycline-resistant *Chlamydia* as described in this work were reviewed and approved by the National Institutes of Health Recombinant DNA Advisory Committee (University of Washington). Recombination experiments were performed as previously described (47). Briefly, sets of individual shell vias were seeded with McCoy cells and subsequently coinfecting with the following combinations of

drug-resistant strains: *C. trachomatis* L1/*tet*^r (NCBI accession number [ACU101000000](https://doi.org/10.1093/nar/32/1/ACU101000000)), *C. trachomatis* serovar F/*tet*^r, and either *C. trachomatis* LGV2 (*ct383/4::Tn bla*) or *C. trachomatis* LGV2 *ct339::Tn bla*. Cultures were incubated for 40 h postinfection in the absence of antibiotics and were then detached using $-80^{\circ}\text{C}/37^{\circ}\text{C}$ freeze-thaw. Recombinants were isolated by infection of 96 new shell vial monolayers with 1 ml freeze-thaw lysates and treatment with both penicillin and tetracycline and were passaged until dually resistant clones were detected. Recombinant clones were propagated and cloned by limiting dilution and subsequently evaluated for identification of serovar-specific OmpA. DNA from clones was harvested and subjected to WGS as described above.

Data accessibility. Completed sequences were submitted to GenBank and assigned the following accession numbers (shown in parentheses): *CT015::Tn* (NHAT01000000); *CT036::Tn* (NHAU01000000); *CT153::Tn* (NHAV01000000); *CT333::Tn* (NHAW01000000); *CT339::Tn* (NHAX01000000); *CT392::Tn* (NHAY01000000); *CT550::Tn* (NHAZ01000000); *CT819::Tn* (NHBA01000000). The pCMA vector was completely sequenced and deposited (GenBank accession no. MN177722).

SUPPLEMENTAL MATERIAL

Supplemental material for this article may be found at <https://doi.org/10.1128/mBio.01343-19>.

FIG S1, PDF file, 0.1 MB.

FIG S2, PDF file, 1.7 MB.

FIG S3, PDF file, 0.3 MB.

FIG S4, PDF file, 0.2 MB.

FIG S5, PDF file, 0.2 MB.

TABLE S1, PDF file, 0.2 MB.

ACKNOWLEDGMENTS

We are highly appreciative of constructive feedback and assistance from Kevin Hybiske (University of Washington) and Daniel Rockey (Oregon State University). We are appreciative of Michael Starnbach and Rebeccah Lijek (Harvard University) for guidance and adaptation with respect to the transcervical animal model. We thank David J. Lampe (Duquesne University) for providing the C9 hyperactive transposase. We acknowledge the contributions of Michael Barta and Gregory Peterson with respect to assistance in characterizing *ct015::Tn*, *ct339::Tn*, *ct392::Tn*, and *ct550::Tn*. We are grateful for the efforts of Nancy Schwarting with respect to mouse infections and organ isolations.

S.D.L., Z.E.D., K.S.H., S.B., R.J.S., and P.S.H. were funded by NIH (AI126785). J.W. and P.S.H. were supported by NIH AI125929. P.S.H. was also supported by P20GM113117. Support for genomic sequencing was supplemented by P20GM103638.

REFERENCES

- Picardeau M. 2010. Transposition of fly mariner elements into bacteria as a genetic tool for mutagenesis. *Genetica* 138:551–558. <https://doi.org/10.1007/s10709-009-9408-5>.
- Hamer L, DeZwaan TM, Montenegro-Chamorro MV, Frank SA, Hamer JE. 2001. Recent advances in large-scale transposon mutagenesis. *Curr Opin Chem Biol* 5:67–73. [https://doi.org/10.1016/S1367-5931\(00\)00162-9](https://doi.org/10.1016/S1367-5931(00)00162-9).
- Lampe DJ, Akerley BJ, Rubin EJ, Mekalanos JJ, Robertson HM. 1999. Hyperactive transposase mutants of the Himar1 mariner transposon. *Proc Natl Acad Sci U S A* 96:11428–11433. <https://doi.org/10.1073/pnas.96.20.11428>.
- Keravala A, Liu D, Lechman ER, Wolfe D, Nash JA, Lampe DJ, Robbins PD. 2006. Hyperactive Himar1 transposase mediates transposition in cell culture and enhances gene expression in vivo. *Hum Gene Ther* 17: 1006–1018. <https://doi.org/10.1089/hum.2006.17.1006>.
- Finnegan DJ. 1992. Transposable elements. *Curr Opin Genet Dev* 2:861–867. [https://doi.org/10.1016/S0959-437X\(05\)80108-X](https://doi.org/10.1016/S0959-437X(05)80108-X).
- Wood DO, Wood RR, Tucker AM. 2014. Genetic systems for studying obligate intracellular pathogens: an update. *Curr Opin Microbiol* 17: 11–16. <https://doi.org/10.1016/j.mib.2013.10.006>.
- Lampe DJ, Churchill ME, Robertson HM. 1996. A purified mariner transposase is sufficient to mediate transposition in vitro. *EMBO J* 15: 5470–5479. <https://doi.org/10.1002/j.1460-2075.1996.tb00930.x>.
- Cheng C, Nair ADS, Indukuri VV, Gong S, Felsheim RF, Jaworski D, Munderloh UG, Ganta RR. 2013. Targeted and random mutagenesis of *Ehrlichia chaffeensis* for the identification of genes required for in vivo infection. *PLoS Pathog* 9:e1003171. <https://doi.org/10.1371/journal.ppat.1003171>.
- Beare PA, Howe D, Cockrell DC, Omsland A, Hansen B, Heinzen RA. 2009. Characterization of a *Coxiella burnetii* ftsZ mutant generated by Himar1 transposon mutagenesis. *J Bacteriol* 191:1369–1381. <https://doi.org/10.1128/JB.01580-08>.
- Newton HJ, Kohler LJ, McDonough JA, Temoche-Diaz M, Crabill E, Hartland EL, Roy CR. 2014. A screen of *Coxiella burnetii* mutants reveals important roles for Dot/lcm effectors and host autophagy in vacuole biogenesis. *PLoS Pathog* 10:e1004286. <https://doi.org/10.1371/journal.ppat.1004286>.
- Clark TR, Lackey AM, Kleba B, Driskell LO, Lutter EI, Martens C, Wood DO, Hackstadt T. 2011. Transformation frequency of a mariner-based transposon in *Rickettsia rickettsii*. *J Bacteriol* 193:4993–4995. <https://doi.org/10.1128/JB.05279-11>.
- Benjamin HW, Kleckner N. 1992. Excision of Tn10 from the donor site during transposition occurs by flush double-strand cleavages at the transposon termini. *Proc Natl Acad Sci U S A* 89:4648–4652. <https://doi.org/10.1073/pnas.89.10.4648>.
- Yahara K, Didelot X, Ansari MA, Sheppard SK, Falush D. 2014. Efficient inference of recombination hot regions in bacterial genomes. *Mol Biol Evol* 31:1593–1605. <https://doi.org/10.1093/molbev/msu082>.
- Sota M, Tsuda M, Yano H, Suzuki H, Forney LJ, Top EM. 2007. Region-specific insertion of transposons in combination with selection for high plasmid transferability and stability accounts for the structural similarity

- of IncP-1 plasmids. *J Bacteriol* 189:3091–3098. <https://doi.org/10.1128/JB.01906-06>.
15. Martinez E, de la Cruz F. 1990. Genetic elements involved in Trn21 site-specific integration, a novel mechanism for the dissemination of antibiotic-resistance genes. *EMBO J* 9:1275–1281. <https://doi.org/10.1002/j.1460-2075.1990.tb08236.x>.
 16. Stephens RS. 1999. *Chlamydia*: intracellular biology, pathogenesis, and immunity. American Society for Microbiology, Washington, DC.
 17. Gottlieb SL. 2010. Summary: the natural history and immunobiology of *Chlamydia trachomatis* genital infection and implications for *Chlamydia* control. *J Infect Dis* 201(Suppl 2):S190–S204. <https://doi.org/10.1086/652401>.
 18. Thomson NR, Holden MTG, Carder C, Lennard N, Lockey SJ, Marsh P, Skipp P, O'Connor CD, Goodhead I, Norbertzack H, Harris B, Ormond D, Rance R, Quail MA, Parkhill J, Stephens RS, Clarke IN. 2007. *Chlamydia trachomatis*: genome sequence analysis of lymphogranuloma venereum isolates. *Genome Res* 18:161–171. <https://doi.org/10.1101/gr.7020108>.
 19. Stephens RS. 1998. Genome Sequence of an Obligate Intracellular Pathogen of Humans: *Chlamydia trachomatis*. *Science* 282:754–759. <https://doi.org/10.1126/science.282.5389.754>.
 20. Gomes JP, Bruno WJ, Borrego MJ, Dean D. 2004. Recombination in the genome of *Chlamydia trachomatis* involving the polymorphic membrane protein C gene relative to *ompA* and evidence for horizontal gene transfer. *J Bacteriol* 186:4295–4306. <https://doi.org/10.1128/JB.186.13.4295-4306.2004>.
 21. Eder T, Kobus S, Stallmann S, Stepanow S, Köhrer K, Hegemann JH, Rattei T. 24 November 2017, posting date. Genome sequencing of *Chlamydia trachomatis* serovars E and F reveals substantial genetic variation. *Pathog Dis* <https://doi.org/10.1093/femspd/ftx120>.
 22. Joseph SJ, Didelot X, Gandhi K, Dean D, Read TD. 2011. Interplay of recombination and selection in the genomes of *Chlamydia trachomatis*. *Biol Direct* 6:28. <https://doi.org/10.1186/1745-6150-6-28>.
 23. DeMars R, Weinfurter J. 2008. Interstrain gene transfer in *Chlamydia trachomatis* in vitro: mechanism and significance. *J Bacteriol* 190:1605–1614. <https://doi.org/10.1128/JB.01592-07>.
 24. DeMars R, Weinfurter J, Guex E, Lin J, Potucek Y. 2007. Lateral gene transfer in vitro in the intracellular pathogen *Chlamydia trachomatis*. *J Bacteriol* 189:991–1003. <https://doi.org/10.1128/JB.00845-06>.
 25. Jeffrey BM, Suchland RJ, Eriksen SG, Sandoz KM, Rockey DD. 2013. Genomic and phenotypic characterization of in vitro-generated *Chlamydia trachomatis* recombinants. *BMC Microbiol* 13:142. <https://doi.org/10.1186/1471-2180-13-142>.
 26. Jeffrey BM, Suchland RJ, Quinn KL, Davidson JR, Stamm WE, Rockey DD. 2010. Genome sequencing of recent clinical *Chlamydia trachomatis* strains identifies loci associated with tissue tropism and regions of apparent recombination. *Infect Immun* 78:2544–2553. <https://doi.org/10.1128/IAI.01324-09>.
 27. Wang Y, Kahane S, Cutcliffe LT, Skilton RJ, Lambden PR, Clarke IN. 2011. Development of a transformation system for *Chlamydia trachomatis*: restoration of glycogen biosynthesis by acquisition of a plasmid shuttle vector. *PLoS Pathog* 7:e1002258. <https://doi.org/10.1371/journal.ppat.1002258>.
 28. Wickstrum J, Sammons LR, Restivo KN, Hefty PS. 2013. Conditional gene expression in *Chlamydia trachomatis* using the *tet* system. *PLoS One* 8:e76743. <https://doi.org/10.1371/journal.pone.0076743>.
 29. Johnson CM, Fisher DJ. 2013. Site-specific, insertional inactivation of *incA* in *Chlamydia trachomatis* using a group II intron. *PLoS One* 8:e83989. <https://doi.org/10.1371/journal.pone.0083989>.
 30. Hooppaw AJ, Fisher DJ. 2015. A coming of age story: *Chlamydia* in the post-genetic era. *Infect Immun* 84:612–621. <https://doi.org/10.1128/IAI.01186-15>.
 31. Bastidas RJ, Valdivia RH. 2016. Emancipating *Chlamydia*: advances in the genetic manipulation of a recalcitrant intracellular pathogen. *Microbiol Mol Biol Rev* 80:411–427. <https://doi.org/10.1128/MMBR.00071-15>.
 32. Ouellette SP. 2018. Feasibility of a conditional knockout system for *Chlamydia* based on CRISPR interference. *Front Cell Infect Microbiol* 8:59. <https://doi.org/10.3389/fcimb.2018.00059>.
 33. Mueller KE, Wolf K, Fields KA. 2016. Gene deletion by fluorescence-reported allelic exchange mutagenesis in *Chlamydia trachomatis*. *mBio* 7:e01817-15. <https://doi.org/10.1128/mBio.01817-15>.
 34. Binet R, Maurelli AT. 2009. Transformation and isolation of allelic exchange mutants of *Chlamydia psittaci* using recombinant DNA introduced by electroporation. *Proc Natl Acad Sci U S A* 106:292–297. <https://doi.org/10.1073/pnas.0806768106>.
 35. Kari L, Goheen MM, Randall LB, Taylor LD, Carlson JH, Whitmire WM, Virok D, Rajaram K, Endresz V, McClarty G, Nelson DE, Caldwell HD. 2011. Generation of targeted *Chlamydia trachomatis* null mutants. *Proc Natl Acad Sci U S A* 108:7189–7193. <https://doi.org/10.1073/pnas.1102229108>.
 36. Kokes M, Dunn JD, Granek JA, Nguyen BD, Barker JR, Valdivia RH, Bastidas RJ. 2015. Integrating chemical mutagenesis and whole-genome sequencing as a platform for forward and reverse genetic analysis of *Chlamydia*. *Cell Host Microbe* 17:716–725. <https://doi.org/10.1016/j.chom.2015.03.014>.
 37. Nguyen B, Valdivia R. 2014. A chemical mutagenesis approach to identify virulence determinants in the obligate intracellular pathogen *Chlamydia trachomatis*. *Methods Mol Biol* 1197:347–358. https://doi.org/10.1007/978-1-4939-1261-2_20.
 38. Hefty PS, Stephens RS. 2007. Chlamydial type III secretion system is encoded on ten operons preceded by sigma 70-like promoter elements. *J Bacteriol* 189:198–206. <https://doi.org/10.1128/JB.01034-06>.
 39. Barta ML, Battaile KP, Lovell S, Hefty PS. 2015. Hypothetical protein CT398 (CdsZ) interacts with sigma(54) (RpoN)-holoenzyme and the type III secretion export apparatus in *Chlamydia trachomatis*. *Protein Sci* 24:1617–1632. <https://doi.org/10.1002/pro.2746>.
 40. Albrecht M, Sharma CM, Reinhardt R, Vogel J, Rudel T. 2010. Deep sequencing-based discovery of the *Chlamydia trachomatis* transcriptome. *Nucleic Acids Res* 38:868–877. <https://doi.org/10.1093/nar/gkp1032>.
 41. Gong S, Yang Z, Lei L, Shen L, Zhong G. 2013. Characterization of *Chlamydia trachomatis* plasmid-encoded open reading frames. *J Bacteriol* 195:3819–3826. <https://doi.org/10.1128/JB.00511-13>.
 42. Song L, Carlson JH, Whitmire WM, Kari L, Virtaneva K, Sturdevant DE, Watkins H, Zhou B, Sturdevant GL, Porcella SF, McClarty G, Caldwell HD. 14 January 2013, posting date. *Chlamydia trachomatis* plasmid-encoded Pgp4 is a transcriptional regulator of virulence-associated genes. *Infect Immun* <https://doi.org/10.1128/IAI.01305-12>.
 43. O'Meara CP, Andrew DW, Beagley KW. 2014. The mouse model of *Chlamydia genital* tract infection: a review of infection, disease, immunity and vaccine development. *Curr Mol Med* 14:396–421. <https://doi.org/10.2174/15665240113136660078>.
 44. De Clercq E, Kalmar I, Vanrompay D. 2013. Animal models for studying female genital tract infection with *Chlamydia trachomatis*. *Infect Immun* 81:3060–3067. <https://doi.org/10.1128/IAI.00357-13>.
 45. Gondek DC, Olive AJ, Stary G, Starnbach MN. 2012. CD4⁺ T cells are necessary and sufficient to confer protection against *Chlamydia trachomatis* infection in the murine upper genital tract. *J Immunol* 189:2441–2449. <https://doi.org/10.4049/jimmunol.1103032>.
 46. Fischer A, Harrison KS, Ramirez Y, Auer D, Chowdhury SR, Prusty BK, Sauer F, Dimond Z, Kisker C, Hefty PS, Rudel T. 28 March 2017, posting date. *Chlamydia trachomatis*-containing vacuole serves as deubiquitination platform to stabilize Mcl-1 and to interfere with host defense. *Elife* <https://doi.org/10.7554/eLife.21465>.
 47. Suchland RJ, Sandoz KM, Jeffrey BM, Stamm WE, Rockey DD. 2009. Horizontal transfer of tetracycline resistance among *Chlamydia* spp. in vitro. *Antimicrob Agents Chemother* 53:4604–4611. <https://doi.org/10.1128/AAC.00477-09>.
 48. Hayes LJ, Yearsley P, Trehan JD, Ballard RA, Fehler GH, Ward ME. 1994. Evidence for naturally occurring recombination in the gene encoding the major outer membrane protein of lymphogranuloma venereum isolates of *Chlamydia trachomatis*. *Infect Immun* 62:5659–5663.
 49. Marti H, Kim H, Joseph SJ, Dojiri S, Read TD, Dean D. 2017. Tet(C) gene transfer between *Chlamydia suis* strains occurs by homologous recombination after co-infection: implications for spread of tetracycline-resistance among *Chlamydiaceae*. *Front Microbiol* 8:156.
 50. Draskovic I, Dubnau D. 2004. Biogenesis of a putative channel protein, ComEC, required for DNA uptake: membrane topology, oligomerization and formation of disulphide bonds. *Mol Microbiol* 55:881–896. <https://doi.org/10.1111/j.1365-2958.2004.04430.x>.
 51. Muschiol S, Balaban M, Normark S, Henriques-Normark B. 2015. Uptake of extracellular DNA: competence induced pili in natural transformation of *Streptococcus pneumoniae*. *Bioessays* 37:426–435. <https://doi.org/10.1002/bies.201400125>.
 52. Nunes A, Nogueira PJ, Borrego MJ, Gomes JP. 2008. *Chlamydia trachomatis* diversity viewed as a tissue-specific coevolutionary arms race. *Genome Biol* 9:R153. <https://doi.org/10.1186/gb-2008-9-10-r153>.
 53. Keb G, Hayman R, Fields KA. 26 November 2018, posting date. Floxed-cassette allelic exchange mutagenesis enables markerless gene deletion

- in *Chlamydia trachomatis* and can reverse cassette-induced polar effects. *J Bacteriol* <https://doi.org/10.1128/JB.00479-18>.
54. Bauler LD, Hackstadt T. 2014. Expression and targeting of secreted proteins from *Chlamydia trachomatis*. *J Bacteriol* 196:1325–1334. <https://doi.org/10.1128/JB.01290-13>.
 55. Iliffe-Lee ER, McClarty G. 1999. Glucose metabolism in *Chlamydia trachomatis*: the ‘energy parasite’ hypothesis revisited. *Mol Microbiol* 33:177–187. <https://doi.org/10.1046/j.1365-2958.1999.01464.x>.
 56. Jelsbak L, Hartman H, Schroll C, Rosenkrantz JT, Lemire S, Wallrodt I, Thomsen LE, Poolman M, Kilstrup M, Jensen PR, Olsen JE. 2014. Identification of metabolic pathways essential for fitness of *Salmonella* Typhimurium in vivo. *PLoS One* 9:e101869. <https://doi.org/10.1371/journal.pone.0101869>.
 57. Sasseti CM, Rubin EJ. 2003. Genetic requirements for mycobacterial survival during infection. *Proc Natl Acad Sci U S A* 100:12989–12994. <https://doi.org/10.1073/pnas.2134250100>.
 58. Martinez E, Cantet F, Fava L, Norville I, Bonazzi M. 2014. Identification of OmpA, a *Coxiella burnetii* protein involved in host cell invasion, by multi-phenotypic high-content screening. *PLoS Pathog* 10:e1004013. <https://doi.org/10.1371/journal.ppat.1004013>.
 59. Misaghi S, Balsara ZR, Catic A, Spooner E, Ploegh HL, Starnbach MN. 2006. *Chlamydia trachomatis*-derived deubiquitinating enzymes in mammalian cells during infection. *Mol Microbiol* 61:142–150. <https://doi.org/10.1111/j.1365-2958.2006.05199.x>.
 60. Le Negrate G, Krieg A, Faustini B, Loeffler M, Godzik A, Krajewski S, Reed JC. 2008. ChlaDub1 of *Chlamydia trachomatis* suppresses NF- κ B activation and inhibits I κ B α ubiquitination and degradation. *Cell Microbiol* 10:1879–1892. <https://doi.org/10.1111/j.1462-5822.2008.01178.x>.
 61. Gerondakis S, Fulford TS, Messina NL, Grumont RJ. 2014. NF- κ B control of T cell development. *Nat Immunol* 15:15–25. <https://doi.org/10.1038/ni.2785>.
 62. Hower S, Wolf K, Fields KA. 15 May 2009, posting date. Evidence that CT694 is a novel *Chlamydia trachomatis* T3S substrate capable of functioning during invasion or early cycle development. *Mol Microbiol* <https://doi.org/10.1111/j.1365-2958.2009.06732.x>.
 63. da Cunha M, Milho C, Almeida F, Pais SV, Borges V, Maurício R, Borrego M, Gomes J, Mota L. 2014. Identification of type III secretion substrates of *Chlamydia trachomatis* using *Yersinia enterocolitica* as a heterologous system. *BMC Microbiol* 14:40–14. <https://doi.org/10.1186/1471-2180-14-40>.
 64. Belland RJ, Zhong G, Crane DD, Hogan D, Sturdevant D, Sharma J, Beatty WL, Caldwell HD. 2003. Genomic transcriptional profiling of the developmental cycle of *Chlamydia trachomatis*. *Proc Natl Acad Sci U S A* 100:8478–8483. <https://doi.org/10.1073/pnas.1331135100>.
 65. Nicholson TL, Olinger L, Chong K, Schoolnik G, Stephens RS. 2003. Global stage-specific gene regulation during the developmental cycle of *Chlamydia trachomatis*. *J Bacteriol* 185:3179–3189. <https://doi.org/10.1128/JB.185.10.3179-3189.2003>.
 66. Gardy JL, Laird MR, Chen F, Rey S, Walsh CJ, Ester M, Brinkman FSL. 2005. PSORTb v.2.0: expanded prediction of bacterial protein subcellular localization and insights gained from comparative proteome analysis. *Bioinformatics* 21:617–623. <https://doi.org/10.1093/bioinformatics/bti057>.
 67. Charpentier X, Faucher SP, Kalachikov S, Shuman HA. 2008. Loss of RNase R induces competence development in *Legionella pneumophila*. *J Bacteriol* 190:8126–8136. <https://doi.org/10.1128/JB.01035-08>.
 68. Baker JA, Simkovic F, Taylor HMC, Rigden DJ. 2016. Potential DNA binding and nuclease functions of ComEC domains characterized in silico. *Proteins* 84:1431–1442. <https://doi.org/10.1002/prot.25088>.
 69. Schultz J, Milpetz F, Bork P, Ponting CP. 1998. SMART, a simple modular architecture research tool: identification of signaling domains. *Proc Natl Acad Sci U S A* 95:5857–5864. <https://doi.org/10.1073/pnas.95.11.5857>.
 70. Hofreuter D, Odenbreit S, Haas R. 2001. Natural transformation competence in *Helicobacter pylori* is mediated by the basic components of a type IV secretion system. *Mol Microbiol* 41:379–391. <https://doi.org/10.1046/j.1365-2958.2001.02502.x>.
 71. Johnston C, Martin B, Fichant G, Polard P, Claverys J-P. 2014. Bacterial transformation: distribution, shared mechanisms and divergent control. *Nat Rev Microbiol* 12:181–196. <https://doi.org/10.1038/nrmicro3199>.
 72. Mukhopadhyay S, Clark AP, Sullivan ED, Miller RD, Summersgill JT. 2004. Detailed protocol for purification of *Chlamydia pneumoniae* elementary bodies. *J Clin Microbiol* 42:3288–3290. <https://doi.org/10.1128/JCM.42.7.3288-3290.2004>.
 73. Suchland RJ, Bourillon A, Denamur E, Stamm WE, Rothstein DM. 2005. Rifampin-resistant RNA polymerase mutants of *Chlamydia trachomatis* remain susceptible to the ansamycin rifalazil. *Antimicrob Agents Chemother* 49:1120–1126. <https://doi.org/10.1128/AAC.49.3.1120-1126.2005>.
 74. Bond SR, Naus CC. 8 May 2012, posting date. RF-Cloning.org: an online tool for the design of restriction-free cloning projects. *Nucleic Acids Res* <https://doi.org/10.1093/nar/gks396>.
 75. Illumina. 2013. MiSeq sample sheet quick reference guide. Illumina, San Diego, CA. https://support.illumina.com/downloads/miseq_sample_sheet_quick_reference_guide_15028392.html.
 76. Seth-Smith HM, Harris SR, Persson K, Marsh P, Barron A, Bignell A, Bjartling C, Clark L, Cutcliffe LT, Lambden PR, Lennard N, Lockey SJ, Quail MA, Salim O, Skilton RJ, Wang Y, Holland MJ, Parkhill J, Thomson NR, Clarke IN. 2009. Co-evolution of genomes and plasmids within *Chlamydia trachomatis* and the emergence in Sweden of a new variant strain. *BMC Genomics* 10:239. <https://doi.org/10.1186/1471-2164-10-239>.
 77. Tatusov RL, Galperin MY, Natale DA, Koonin EV. 2000. The COG database: a tool for genome-scale analysis of protein functions and evolution. *Nucleic Acids Res* 28:33–36. <https://doi.org/10.1093/nar/28.1.33>.
 78. Tusnady GE, Simon I. 2001. The HMMTOP transmembrane topology prediction server. *Bioinformatics* 17:849–850. <https://doi.org/10.1093/bioinformatics/17.9.849>.
 79. Buchan DWA, Ward SM, Lobley AE, Nugent TCO, Bryson K, Jones DT. 2010. Protein annotation and modelling servers at University College London. *Nucleic Acids Res* 38:W563–W568. <https://doi.org/10.1093/nar/gkq427>.
 80. Krogh A, Larsson B, von Heijne G, Sonnhammer ELL. 2001. Predicting transmembrane protein topology with a hidden Markov model: application to complete genomes. *J Mol Biol* 305:567–580. <https://doi.org/10.1006/jmbi.2000.4315>.
 81. Claros MG, von Heijne G. 1994. TopPred II: an improved software for membrane protein structure predictions. *Comput Appl Biosci* 10:685–686. <https://doi.org/10.1093/bioinformatics/10.6.685>.
 82. Juretić D, Zoranić L, Zucić D. 2002. Basic charge clusters and predictions of membrane protein topology. *J Chem Inf Comput Sci* 42:620–632. <https://doi.org/10.1021/ci010263s>.
 83. Omasits U, Ahrens CH, Müller S, Wollscheid B. 24 October 2013, posting date. Protter: interactive protein feature visualization and integration with experimental proteomic data. *Bioinformatics* <https://doi.org/10.1093/bioinformatics/btt607>.